SLOW-STRAIN-RATE-HYDROGEN EMBRITTLEMENT AND STRESS-CORROSION CRACKING IN Ti-Al BINARY ALLOYS

A THESIS

Presented to

The Faculty of the Graduate Division

by

David Alexander Mauney

In Partial Fulfillment

of the Requirements for the Degree

Master of Science in Metallurgy

Georgia Institute of Technology

June, 1969

SLOW-STRAIN-RATE-HYDROGEN EMBRITTLEMENT AND STRESS-CORROSION CRACKING

IN Ti-Al BINARY ALLOYS

Approved:

Chairman

Date approved by Chairman: 6/13/69

ACKNOWLEDGMENTS

The author wishes to express his gratitude to Dr. E. A. Starke, Jr., his thesis advisor, for his encouragement and patience during the course of this project. He also wishes to thank Drs. B. G. LeFevre and R. F. Hochman for reviewing this work.

The author gratefully acknowledges the assistance of Mr. D. A. Meyn and the Naval Research Laboratory for instruction in electron fractography, and Dr. W. E. Krull and the Lockheed-Georgia Company for use of their X-ray diffraction equipment. Special appreciation is expressed to Mr. G. P. Rauscher and the Boeing Company for instruction in the preparation of thin foils for transmission electron microscopy, for charging the project alloys with hydrogen, for analyzing the project alloys, and for very valuable discussions. The author also wishes to thank Drs. J. C. Williams, M. J. Blackburn, and R. M. N. Pelloux for discussing various phases of this project. The support of this project by Advance Research Projects Agency's Order Number 878 of the Department of Defense is greatly appreciated.

Last, but not least, the author is especially grateful to his wife, Louise, and his son, Sam, for their encouragement, patience, and love during these trying times.

TABLE OF CONTENTS

TABLE OF CONTENTS (Continued)

LIST OF TABLES

LIST OF FIGURES

LIST OF FIGURES (Continued)

LIST OF FIGURES (Continued)

SUMMARY

This study was undertaken in an effort to define the possible role of hydrogen in the stress-corrosion cracking (SCC) process. In this regard, the process was studied by comparing fracture characteristics of SCC to slow-strain-rate-hydrogen embrittlement (SSRHE) in three Ti-Al binary alloys (2.5, 5, and 8 weight percent Al) using electron fractography and X-ray diffraction. The deformation characteristics of SSRHE in these three alloys were studied using thin foil transmission electron microscopy.

The similarities between SCC and SSRHE failures in Ti-5 and 8 weight percent Al alloys strongly suggest that hydrogen plays a significant role in the SCC process. The present observations indicate that the precipitation of hydrides on coplanar dislocations is related to the mode of SCC and SSRHE failure in Ti-Al alloys. The cleavage habit plane observed for SCC, which is close to but not the basal plane, appears to be the prominent fracture plane for all brittle failures of these Ti-Al binary alloys.

CHAPTER I

INTRODUCTION

The growing requirements on high-strength materials for spacecraft, deep-sea diving vessels, and high-speed aircraft have caused particular attention to be paid to their weaknesses, one of which is their possible susceptibility to stress-corrosion cracking (SCC)[1]. Since Ti-base alloys are used to a large extent for these applications, the detection by Brown[2] of the susceptibility in some Ti alloys to SCC in room temperature 3.5 percent NaCl solution has had a large impact on their uses. Much effort has been put forth to offer an explanation for this phenomenon.

Investigations in the Ti-8 weight percent Al-1 weight percent Mo-1 weight percent V (Ti-8-1-1) alloy have shown that the hexagonal-closed-packed (hcp) α-phase is the susceptible phase[3]. Considering this result, Blackburn and Williams[4] studied the effect of Al concentration on SCC of binary α-phase alloys in a room temperature-chloride solution and found the susceptibility to increase with Al content. However, the reasons for the increase in susceptibility are not clearly understood. In fact, none of the present theories explain all the characteristics of SCC in room temperature 3.5 percent NaCl solution.

There is much disagreement in the literature concerning the possible role of hydrogen in the SCC process. In addition, there are several similarities between slow-strain-rate-hydrogen embrittlement (SSRHE) and

SCC in Ti alloys which should be considered[1]. A review of certain earlier work is necessary before any definitive experiments can be proposed to investigate the similarities of these two processes.

Ti-Al System

Aluminum is the most important alloying element for Ti since on a weight percentage basis it produces the greatest strengthening effect[5]. Aluminum is also an α-phase stabilizer (i.e., it increases the α-β transition temperature) and has a greater solubility in the α-phase than the β-phase[6].

The Ti-Al phase diagram was first developed by Ogden, Maykuth, Finlay, and Jaffee[7] and later confirmed by Bumps, Kessler, and Hansen[8]. Their diagrams showed an α-phase field up to 25 weight percent Al. Later work[9-13] showed that in the α-phase field an ordering reaction occurs which results in an ordered Ti_3Al phase with DO_{19} type structure.

It is impossible to retain the β-phase on quenching Ti-Al alloys[14]. The β to α transformation is diffusionless[15] and results in needles containing a high density of dislocations. This same transformation appears in pure Ti[16] which has the Burger's orientation relationship to prior β phase[17,18].

The long controversy over the Ti-rich end of the Ti-Al phase diagram[19] has had several contributing factors. Dwelling in the α+β phase field during heat treatment or hot working can result in partitioning of Al between these two phases. Subsequent cooling to room temperature results in a nonhomogeneous α-phase that gives the appearance of a two-phase field when using both X-ray diffraction and bright-field-light

microscopic techniques[20]. At low Al content small Ti_3Al particles cannot be resolved by light microscopy, even after long aging times[19]. In addition, Ti hydrides[19] or surface expansions due to hydrogen[21] can be introduced by etching[19,21,22], obscuring the true structure of the alloy. X-ray diffraction data can be misinterpreted because of increases in the α-lattice parameters due to hydrogen[21,22]. These anomalies occur in both ordered and disordered alloys[19].

Blackburn[19], using thin foil transmission electron microscopy and X-ray diffraction, has been able to circumvent the above mentioned difficulties. The phase diagram determined by him, Figure 1, shows good agreement with those of several other workers[9,23-25] for 0 to 15 atomic percent Al content. Blackburn's phase diagram for the Ti-rich end of the Ti-Al system has the general form found in systems having solid state order-disorder transformations. On this diagram α is the disordered hcp phase and α_2 the ordered phase. From 0 to 15 atomic percent Al, the structure goes from the disordered α-phase through short-range order, to small ordered domains in a disordered α-matrix[19]. For purposes of this investigation, Blackburn's phase diagram will be used for this region.

Ti-Al-H System

Hydrogen is an exothermic interstitial occluder with Ti, because there is a complication by the formation of a hydride phase[26]. The Ti-H phase diagram, above 450°C, was determined by McQuillan[27] using pressure-temperature measurements at constant volume. Lenning, Craighead, and Jaffee[28], in studies below 400°C, showed the solubility of hydrogen

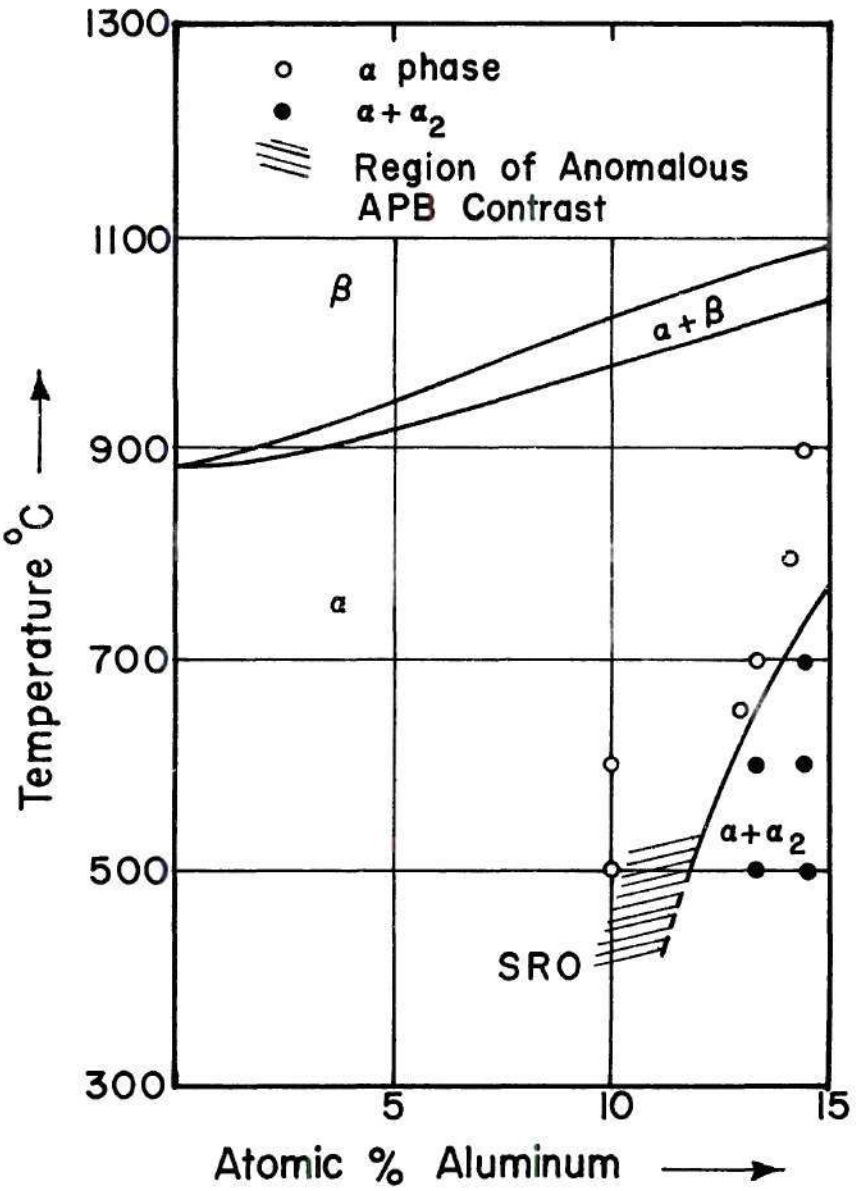

Figure 1. The Titanium-Aluminum Phase Diagram from 0 to 15 Atomic Percent Al (after Blackburn[19])

to be 1400 parts per million (ppm) at 300°C, dropping to 10 to 29 ppm at 125°C and remaining constant to room temperature.

Berger, Williams, and Jaffee[29] have determined the room temperature Ti-Al-H isotherm by light metallography and impact testing. Their diagram suggested that increasing Al content increased hydrogen solubility. However, further investigation of the strained region of a "single phase" alloy tensile specimen showed hydrides. This evidence suggested that Al retards the rate of hydride precipitation instead of increasing hydrogen solubility for hydrogen introduced at elevated temperatures. Boyd[30], using thin foil transmission electron microscopy, also showed that increasing the Al content in a Ti alloy inhibits Ti hydride formation, but that Al does not appreciably change the equilibrium solubility of hydrogen in Ti.

Experimental difficulties in the determination of the Ti-Al-H system arise for several reasons; for example, the high temperature single phase structure can either not be retained upon quenching or hydrides are precipitated at room temperature[6,31]. Just as in Ti-Al alloys, a false expansion structure can result from hydrogen pick-up at the surface. This structure depends on Al content and etching time. Increased amounts of Ti_3Al[22] and certain etchants, causing effective hydrogen pressures of many thousand of atmospheres[32], can result in increased absorption of hydrogen. Sufficient hydrogen for hydride precipitation may result. The false hydrogen structure can be circumvented by use of transmission electron microscopy on thin foils prepared by the technique used by Blackburn and Williams[33].

Titanium hydride (TiH_2), a stoichiometric compound containing

66.6 atomic percent hydrogen[27], was found by several investigators[28,34] to be of face-centered-cubic (fcc) structure, while another found it to be tetragonal[35]. This inconsistency was clarified by Yakel[36] who noted Ti hydrides to be of body-centered-tetragonal (bct) structure below 310°K and fcc above this temperature. The average size of the Ti-hydride-lamella precipitate[19] increases with Al content, for chemically charged hydrogen, suggesting that Al aids the atomic rearrangements necessary for hydride formation[34]. Titanium hydrides have been reported to form predominantely on $\{10\bar{1}0\}$ and $\{10\bar{1}1\}$ planes of the hcp α-matrix[19,34] which are two of the possible slip planes in Ti and Ti-Al alloys[37].

Modes of Deformation in the Ti-Al System

The most prevalent slip systems in Ti are $\{10\bar{1}0\}1/3 < 11\bar{2}0 >$, $\{10\bar{1}1\}1/3 < 11\bar{2}0 >$, and $(0001)1/3 < 11\bar{2}0 >$. Less prominently found is $\{11\bar{2}2\}1/3 < 11\bar{2}3 >$[38]. As Al is added, $\{10\bar{1}0\}1/3 < 11\bar{2}0 >$ becomes preferred and $\{10\bar{1}1\}1/3 < 11\bar{2}0 >$[39] and $\{11\bar{2}2\}1/3 < 11\bar{2}3 >$[38] are less active. Below approximately 5 weight percent Al, dislocations lie in a cellular arrangement of tangles, whereas above this amount they lie in well defined coplanar arrays[4]. In alloys above 6 weight percent Al basal slip is only found after high strains[40].

The texture of cold-rolled pure Ti is not typical of hcp metals. When more than 1.4 weight percent Al is added, however, it changes to one of a typical hcp metal, $(0001)\ [10\bar{1}0]$. It is thought that the pure Ti texture is due to twinning on the pyramidal planes and that adding Al suppresses this deformation mode leaving slip predominant[5].

Slow-Strain-Rate-Hydrogen Embrittlement in the Ti-Al-H System

Slow-strain-rate-hydrogen embrittlement is caused by a decrease in solid solubility of hydrogen in the α-phase Ti alloys. If precipitation is suppressed during cooling, a supersaturated solid solution remains that is susceptible to SSRHE since either hydride precipitation or hydrogen segregation can occur with straining[32].

In general, for metals that suffer SSRHE, the overload-fast-fracture stress after slow-crack propagation in hydrogen-charged specimens is the same as the overload-fast-fracture stress of noncharged specimens. This could mean that the average hydrogen concentration in a charged specimen is not enough to cause slow-crack propagation necessitating a hydrogen build-up in the highly stressed region ahead of the crack tip before propagation. The following mechanism might be active: when the hydrogen concentration reaches a critical value, cracks are initiated which join the main crack. Crack propagation stops when the crack has left the hydrogen built-up region and must reinitiate before further propagation. This implies a discontinuous process consisting of a series of crack initiations whose rate is controlled by the rate of hydrogen diffusion. Evidence of this discontinuous process has been seen in other metals by the electrical resistance technique[41]. Slow-strain-rate-hydrogen embrittlement is most common in α-β Ti alloys and has been observed in α alloys[32], which exhibit some of these characteristics[41].

The cause of SSRHE in Ti alloys is not known, but the process is very time-dependent. The implication of hydrogen diffusion as the rate controlling process is further substantiated because specimen damage is

not apparent until a crack begins to form. Thus, SSRHE in Ti alloys can be caused by either a critical hydrogen content in solution near the fracture path, or precipitation of hydrides in this area[32]. More specifically, Boyd[30] suggested that strain induced hydrides form during plastic deformation of a Ti alloy susceptible to SSRHE by showing that hydrides formed on the slip planes of a large volume-fraction α-phase Ti-8-1-1 alloy after plastic straining. Williams and Jaffee[42] found signs of SSRHE in a Ti-5 weight percent Al alloy, containing 150 ppm hydrogen, where the strain induced hydride precipitation occurred in the notch of a stress rupture specimen. This occurred although hydrogen embrittlement was not indicated by the time to failure. It is important to emphasize that once hydride platelets are formed microcracks can initiate at the stress concentrations on the sharp edges of the plates or at the head of dislocation pile-ups caused by these platelets[26]. However, no definite proof of the hydride causing the embrittling phenomena has been obtained.

Stress-Corrosion Cracking of Ti-Al Alloys

Stress-corrosion cracking can be defined as a cracking process that is caused by the simultaneous application of a corrodent and sustained tensile stress[43]. The advantage of such a general definition is that it can be applied to a metal corrodent system without knowledge of the fundamental mechanism[44]. Certain Ti-Al alloys are susceptible to SCC under stress in room temperature-chloride solutions in the presence of a notch or other stress risers[4]. The minimum stress for SCC is always less than the overload-fast-fracture stress in air with

the same stress concentration[45]. This cracking occurs if the Al content is approximately 5 weight percent or greater and does so by cleavage on planes approximately 12°-14° to the basal plane in Ti-8 weight percent Al alloy. The planes appear to possibly be of the $\{10\bar{1}7\}$ or $\{10\bar{1}8\}$ type[4].

At the present time no experimental model[40,46-48] explains all the characteristics of SCC of α-phase Ti-Al alloys in 3.5 percent NaCl solution. This study was undertaken in an effort to define the possible role of hydrogen in the SCC process. In this regard, the fracture characteristics in Ti-2.5,5, and 8 weight percent Al alloys under SCC and hydrogen charged conditions will be compared. Electron fractography and X-ray techniques will be used for fracture characterization, and thin foil transmission electron microscopy will be used to study the deformation characteristics of SSRHE. Similar characteristics for SCC and SSRHE should be seen if hydrogen plays a major role in the former process.

CHAPTER II

EXPERIMENTAL PROCEDURE

Specimen Preparation

Alloy Preparation

Titanium-aluminum binary alloys for this study were prepared by Reactive Metals, Inc. using Ti sponge and 99.8 weight percent pure Al shot. Three alloys of 2.5, 5, and 8 weight percent (4.5, 8.2, and 12.9 atomic percent, respectively) Al were vacuum melted, then pressure melted under an argon atmosphere (see Table 1). The resulting ingots were hot rolled in the $\alpha+\beta$ phase field. The scale and oxidized layer were removed by shot blasting, grinding, and HNO_3-HF bath pickling. The final plate sizes were approximately 30 inches long, 5.75 inches wide, and 0.25 inches thick. From these were sheared three specimens of each alloy, 5.75 inches long, 1.575 inches wide, and 0.25 inches thick.

Heat Treatment

These specimens were chemically cleaned in a bath of two parts HF and three parts HNO_3 for 30 seconds at a temperature of $2^{\circ}C$. Each was then water rinsed, acetone dried, and individually wrapped in cleaned Ta foil.

Homogenization. Each specimen was homogenized to remove the Al partitioning that occurred in hot rolling and to allow β grain growth, that would give large α martensite needles on β-quenching[49]. This heat

Table 1. Alloy Compositions

Nominal Alloy (Weight Percent)	Al Content (Weight Percent)	Fe Content (Weight Percent)	C Content (Weight Percent)
Ti-2.5% Al	2.57	0.027	0.02
Ti-5% Al	4.81	0.039	0.01
Ti-8% Al	7.69	0.034	0.03

treatment consisted of holding each specimen at 1400 ± 20°C for 6 hours in a high-temperature-inert-atmosphere-quench furnace and then quenching in water at 55°C (see Appendix). The resulting prior β grain size can be seen in Figure 2. One of the Ti-5 weight percent Al specimens had to be homogenized at 1200°C for 8 hours instead, because of a failure in the furnace tube. The specimen was protected by encapsulating in a quartz tube at a pressure of 3×10^{-5} torr.

Before specimen machining, the oxide was removed by a chemical-mechanical process. Each specimen was submerged in the same cleaning bath as before, which was held below 15°C to keep hydrogen pick-up minimal, and periodically removed for grinding. They were then rinsed and acetone dried. The specimens were machined into single-edge-notch-cantilever-beam specimens to dimensions of 5.75 inches long, 1 inch wide, and 0.25 inches thick with a 0.2 inch deep, 60° included angle notch at their midsections (see Figure 2)[50].

Annealing. Each specimen was prepared for annealing by cleaning in benzene, rinsing in acetone, and encapsulating in groups of not more than five in the vycor end of a vycor-quartz tube at a pressure of 3×10^{-5} torr. Specimens were separated by 0.005 inch tungsten wire spacers. At the quartz end of this evacuated tube were Ti-8-1-1 alloy chips that had been degreased in trichloroethylene, rinsed in acetone, and vacuum cleaned at 500°C until a pressure of 10^{-4} torr was reached.

To anneal out the high dislocation density in the α martensite needles and allow α grain coarsening, the specimens were annealed just under the α transus[48]. The end of the tube containing the titanium alloy chips was placed in one furnace and the specimen end in another.

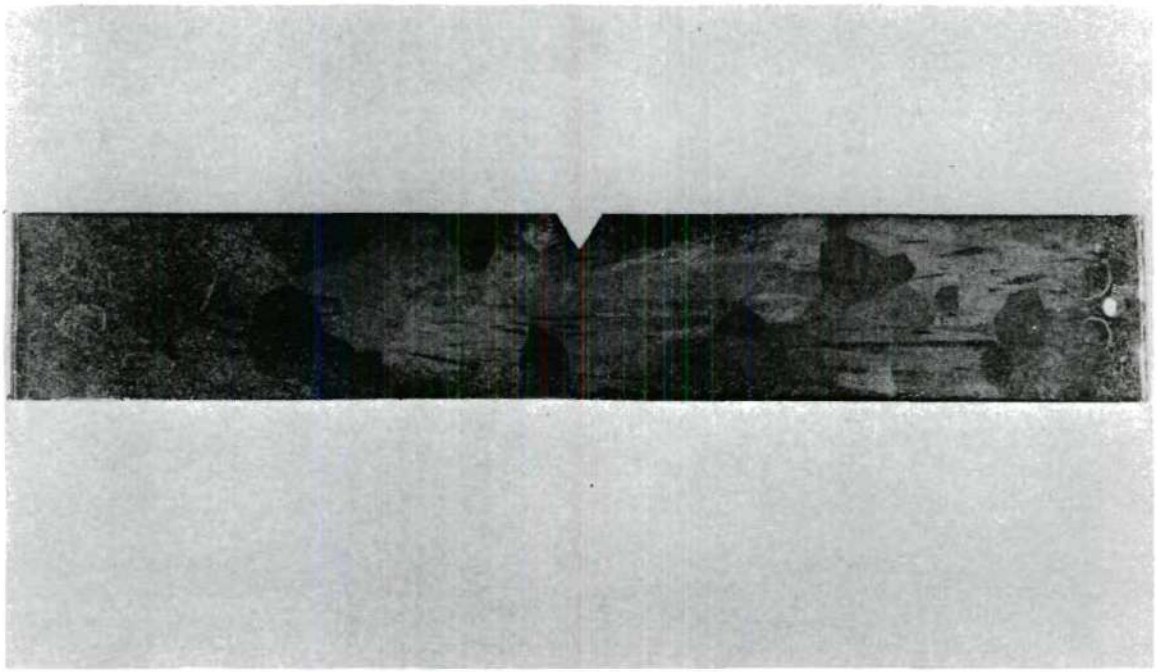

Figure 2. Typical Single-Edge-Notch-Cantilever-Beam Specimen Used in This Study (note large prior β grain size from homogenization at 1400°C, magnification 1X)

The chips were held at 850°C for approximately 18 hours while the specimens were held at 500°C for approximately the last 14 hours. The specimens were then heated and held at 850°C for 168 hours while the chips were held at 950°C. The specimens were slow cooled to 500°C and held for 1 hour to allow them to approach equilibrium. Both ends of the tube were then air-cooled while the specimens and chips remained in a vacuum.

Control of Hydrogen Content

As suggested in Chapter I, there appears to be a critical hydrogen content (or a critical supersaturation of hydrogen) for each Al content and when this critical content is exceeded, hydride precipitation occurs. This critical hydrogen content appears not to be the solubility limit for a particular Al content but the point where that quantity of Al can no longer inhibit hydride precipitation. To test SSRHE susceptibility one specimen of each alloy had its hydrogen content brought to approximately two-thirds that of the critical hydrogen content for that alloy. The hydrogen content was made as low as possible in the other two specimens of each alloy for SCC and laboratory air testing.

Ti-2.5 Weight Percent Al Alloy. The as-heat-treated Ti-2.5 weight percent Al alloy specimens were found to contain approximately 109 ppm hydrogen. Since the critical hydrogen content for this alloy is 380 ppm[51], the specimen for SSRHE susceptibility testing was tested as-heat-treated. The hydrogen content was lowered in the other two specimens by vacuum annealing in a modified Sievert's apparatus. This was accomplished by annealing these two specimens one at a time at 800°C for 6 hours and 10 minutes at a pressure of approximately 10^{-5} torr. The

specimens were slow cooled under vacuum to 500°C, held for 1 hour, and then water quenched.

Ti-5 Weight Percent Al Alloy. The as-heat-treated specimens of Ti-5 weight percent Al contained approximately 140 ppm hydrogen. The critical hydrogen content for this alloy is 425 ppm[51]. The SSRHE susceptibility specimen was charged to 300 ppm hydrogen in the above mentioned Sievert's apparatus. The specimen was vacuum annealed at 800°C for 10 minutes at a pressure of 10^{-5} torr, then purified hydrogen was added at an initial pressure of 49 torr. The specimen was held at this temperature in this atmosphere for 6 hours. The specimen was slow cooled under this atmosphere to 500°C, held for 1 hour, and water quenched. The other two specimens were tested at the as-heat-treated hydrogen content.

Ti-8 Weight Percent Al Alloy. The Ti-8 weight percent Al alloy as-heat-treated specimens contained approximately 125 ppm hydrogen, while the critical hydrogen content for this alloy is 650 ppm[51]. Two of the specimens were tested at the as-heat-treated hydrogen content while the SSRHE susceptibility specimen was charged by the same process as the Ti-5 weight percent Al alloy specimen, except an initial hydrogen pressure of 96 torr was used for a hydrogen content of 590 ppm. The other two specimens were tested at the as-heat-treated hydrogen content.

Specimen Testing

Measuring of the Specimens

Specimen dimension measurements were taken in order to calculate the K_{Ix} (stress intensity factor of the specimen at failure)[2]. First,

a sharp scribe was drawn across the root of the machined notch to sharpen the notch. Next, the notch depth was obtained by measuring the image of the specimen on the frosted glass plate of a Baush and Lomb Macro Camera at a magnification of five times. The notch tip radius of curvature was measured by using the graduated microscope on a Vickers-Armstrong Pyramide Hardness Tester. Micrometers were used for width and thickness measurements.

Fracturing of the Specimens

All specimens were rinsed in benzene and acetone, dried before fracturing, and failed in a standard cantilever-beam machine[2] with a 36-inch moment arm, Figure 3a. The notch was always placed 0.25 inches from the rigid support as shown in a close-up view of the specimen-load configuration in Figure 3b. Each specimen was initially loaded to a K_I (stress intensity factor)[2] of approximately 25,000 psi $\sqrt{\text{in}}$ (pounds per square inch times the square root of inches) and then the load increased approximately 1 pound every 2 minutes until failure.

The grouping of test alloy-environment combinations were as follows: A specimen of low and high hydrogen content of each Ti-Al alloy was failed in laboratory air to compare the effect of varying hydrogen content on different Al content alloys. A specimen of low hydrogen content of each Ti-Al alloy was failed at room temperature in a solution of 3.5 weight percent NaCl in distilled water to compare the SCC process to the SSRHE process at different Al contents. The solution was held around the specimen at the notch by a small polyethylene cup sealed to the specimen with Dow Corning Silastic RTV 731 Adhesive-Sealent which had dried 20 hours.

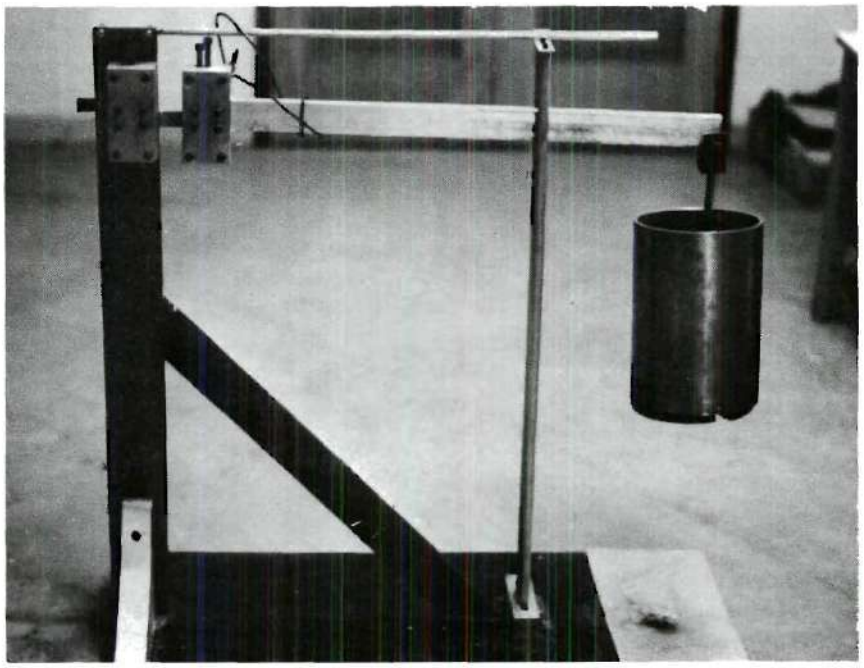

(a)

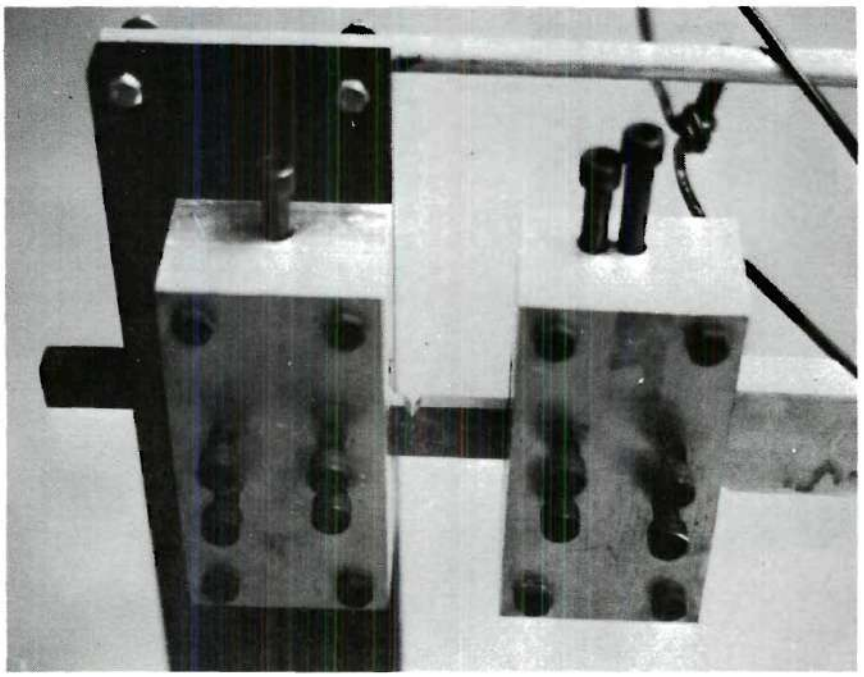

(b)

Figure 3. Standard Cantilever-Beam Machine: (a) General View, (b) View of Specimen-Load Configuration

X-ray Diffraction

Characterization of the brittle fracture habit plane was accomplished by determining the orientation of a suitable number of facets in each macrobrittle fracture specimen using the back-reflection Laue technique. The fracture faces were mounted on a Rigaku Micro Camera which was on a Phillips Norelco X-ray Generator with a Cu target used for the source. The Cu tube was set at 50 KV and 20 mA for an exposure time of 2.5 hours. With the 160 power modified Olympus stereoscope mounted on the micro Laue camera, it was possible to align the approximately 0.2 mm diameter facets perpendicular to the X-ray beam. This was accomplished by changing the orientation of the fracture face until all the facet came in and went out of focus simultaneously as the focusing knob was turned. A 100 μ (micron) collimator was used with an approximate specimen-to-film distance of 5 millimeters.

For ease of indexing, the X-ray films (23 mm by 25 mm) were enlarged and printed on 8 x 10 inch photographic paper to be of a size equal to a specimen-to-film distance of 3 centimeters. This was done so that standard Greninger and stereographic charts could be used in indexing the spots to within $\pm 2^{\circ}$ by standard techniques[52,53].

Electron Microscopy

Fractography

To compare the fracture topography of the different specimens, two replicas were made from the macrobrittle portion and one from the macroductile portion of each brittle specimen. When the whole specimen failed macroductile, one replica was made from the top portion and

another from the bottom portion of the fracture surface. All replicas were made by the two-stage-plastic-carbon technique using cellulose acetate tape for the first stage and Pt-shadowed carbon for the second stage[54]. Approximately four micrographs of each replica were taken using a Siemens Elmiskop IA at 50 KV with projector pole piece V inserted.

Thin Foils

The effect of low and high hydrogen content on the deformation characteristics of the three Ti-Al alloys was investigated by thin foil transmission electron microscopy. Tensile specimens (Figure 4), 0.125 inch thick, were machined from one end of the fractured specimen of each Ti-Al alloy with low and high hydrogen content. The surfaces of these tensile specimens were glycerin ground through 600 grit paper to remove surface roughness. Each specimen was then plastically strained about 5 percent (except the Ti-8 weight percent Al alloy specimen, which failed in the elastic region) at a strain rate of approximately 0.007 inch per inch per minute on an Instron Tensile Machine. Coupons 0.5 inch by 0.5 inch by 0.125 inch were spark-cut from these specimens and then wet ground to a wedge with a slope of 0.005 inch to 0.001 inch thick over a half inch using 180, 220, and 600 grit paper. These wedges were electropolished using the technique described by Blackburn and Williams[33].

Thin foils were examined by transmission electron microscopy in a Siemens Elmiskop IA at 100 KV with projector pole piece III and a Swann stage with $\pm 23^{\circ}$ tilt in two directions. Three micrographs with associated diffraction patterns were taken of each specimen. Slip plane trace analysis was attempted by standard techniques[55-57], but because of inaccuracies in the method, it was impossible to distinguish between

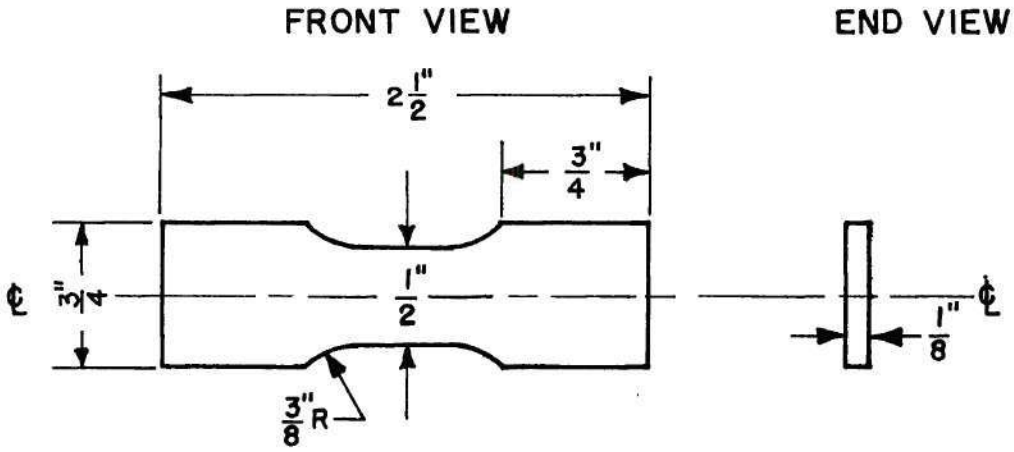

Figure 4. Drawing of Tensile Specimen for Plastic Straining

the four operating slip systems with any degree of certainty. The principal error in trace analysis arises from the fact that the foil surface is generally not perpendicular to the incident beam. The error can be eliminated if the tilt axis of the foil is made coincident with the trace being observed[57]. Since the Swann stage does not allow rotation of the specimen in its plane, this adjustment could not be made.

Gas Analysis

Two samples (approximately 5 grams each) were spark-cut from each fractured specimen for gas analysis. These samples were ground on an 80 grit belt to remove surface contamination. One sample was analyzed for hydrogen content by the hot extraction method[58] and the other for oxygen content by neutron activation[51].

CHAPTER III

RESULTS

The possible role of hydrogen in the SCC process was studied by comparing fracture characteristics of SCC to SSRHE in three Ti-Al binary alloys using electron fractography and X-ray diffraction. The deformation characteristics of SSRHE in these three alloys were studied using thin foil transmission electron microscopy. The alloy-environment combinations are shown in Table 2 along with the K_{Ix} failure values, and hydrogen and oxygen contents of each specimen.

The K_{Ix} used here is only an approximation since the notch tip radii were not sharp (actual radii $\sim$ 0.002 inch), and the grain size of the specimens was large ($\sim$ 2 mm for all except the Ti-5 weight percent Al sample homogenized at 1200°C, which was $\sim$ 0.1 mm). These conditions are contrary to those used in the theoretical development of K_{Ix}[59]. The large grain size allowed the plane strain condition to be satisfied even tough the specimens were only 0.25 inch wide. The K_{Ix} value determined for the Ti-2.5 weight percent Al alloy specimens indicated that the samples were not susceptible to either SCC or SSRHE, even though the latter was observed. On the other hand, a very significant decrease of K_{Ix} was observed for the Ti-5 weight percent Al alloy during SCC in a 3.5 percent NaCl solution. A similar decrease was observed for this alloy during SSRHE. Corresponding results were obtained for the Ti-8 weight percent Al alloy. However, the K_{Ix} for the laboratory-

Table 2. Specimen Alloy-Environment Combinations Showing Stress Intensity Factor at Failure (K_{Ix}), and Specimen Hydrogen and Oxygen Contents

Alloy (Weight Percent)	Laboratory-Air (Low-Hydrogen Content Specimen)	3.5% NaCl Solution (Low-Hydrogen Content Specimen)	Laboratory-Air (High-Hydrogen Content Specimen)
Ti-2.5% Al	K_{Ix} - 63,400 psi $\sqrt{in}$ Hydrogen - 40 ppm Oxygen - 1190 ppm	K_{Ix} - 53,800 psi $\sqrt{in}$ Hydrogen - 27 ppm Oxygen - 1270 ppm	K_{Ix} - 58,600 psi $\sqrt{in}$ Hydrogen - 109 ppm Oxygen - 860 ppm
Ti-5% Al	K_{Ix} - 92,600 psi $\sqrt{in}$ Hydrogen - 137 ppm Oxygen - 1360 ppm	K_{Ix} - 57,800 psi $\sqrt{in}$ Hydrogen - 144 ppm Oxygen - 1520 ppm	K_{Ix} - 63,800 psi $\sqrt{in}$ Hydrogen - 300 ppm Oxygen - 1220 ppm
Ti-8% Al	K_{Ix} - 54,000 psi $\sqrt{in}$ Hydrogen - 132 ppm Oxygen - 920 ppm	K_{Ix} - 37,800 psi $\sqrt{in}$ Hydrogen - 119 ppm Oxygen - 780 ppm	K_{Ix} - -------- ppm $\sqrt{in}$ Hdyrogen - 590 ppm Oxygen - 1470 ppm

air, high-hydrogen content specimen could not be calculated because the specimen failed outside the notch. The failure load was well below the laboratory-air, low-hydrogen failure load indicating susceptibility to SSRHE.

Fracture Surface Characterization

Light and Electron Fractography

Ti-2.5 Weight Percent Al Alloy. The light macrograph of the laboratory-air, low-hydrogen fracture surface, Figure 5a, appears to be an all-ductile failure except for the flat facet denoted by a circle. Electron fractography of this surface showed dimples, Figure 6a, and serpentine glide, Figure 6b, typical of a ductile failure[54]. The one or two flat facets on this specimen showed very small shallow dimples, Figure 7, indicating a low ductility failure[60] in this grain. The same fracture features were observed in the 3.5 percent NaCl solution failure, Figure 5b and Figures 8a and 8b. The whole fracture surface of the laboratory-air, high-hydrogen content specimen was characterized by small flat facets containing river patterns and separated by shear ridges as shown in the light macrograph, Figure 5c, and electron fractographs, Figures 9a and 9b. The river patterns of these flat facets are typical of brittle failure[54].

Ti-5 Weight Percent Al Alloy. The all-ductile appearance of the light macrograph of the Ti-5 weight percent Al alloy, laboratory-air, low-hydrogen content specimen, Figure 10a, is confirmed by the dimples shown in the electron fractographs of this surface, Figure 11a and 11b. However, the 3.5 percent NaCl solution, low-hydrogen failure specimen

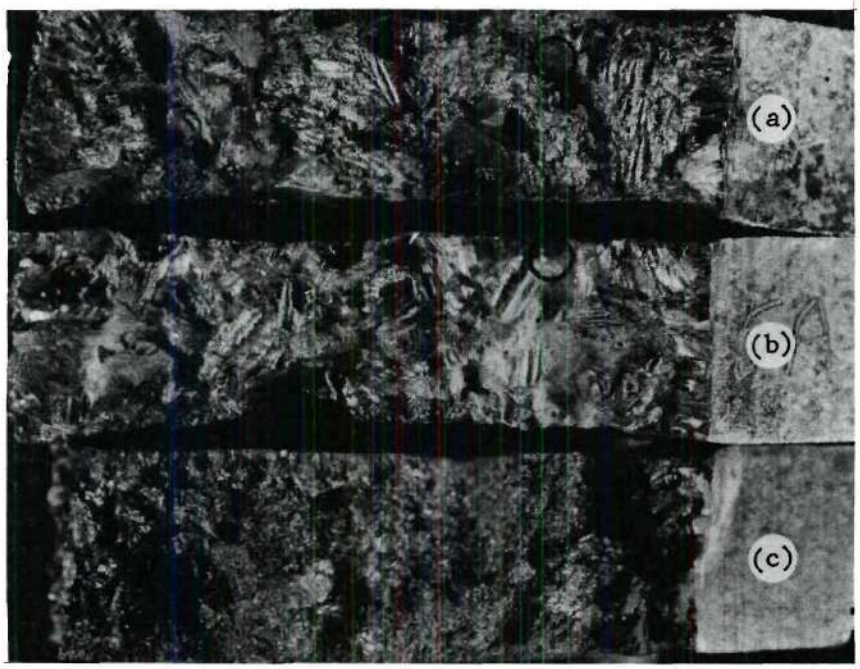

Figure 5. Light Macrographs of the Ti-2.5 Weight Percent Al Alloy Fracture Surfaces: (a) Laboratory-Air, Low-Hydrogen Failure, (b) 3.5 Percent NaCl Solution, Low-Hydrogen Failure, (c) Laboratory-Air, High-Hydrogen Failure (Typical flat facets are circled, notch at right, crack propagation from right to left, magnification 4X)

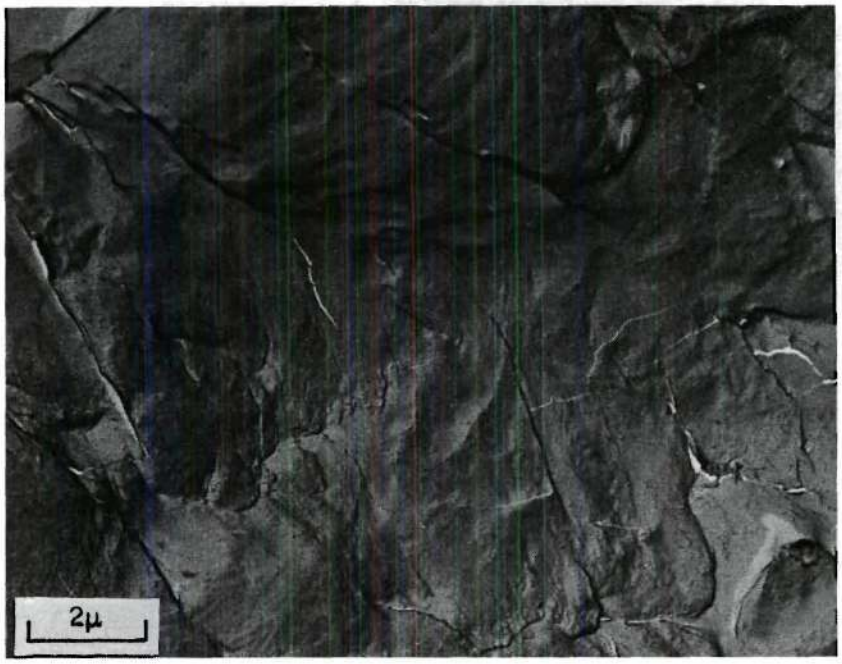

(a)

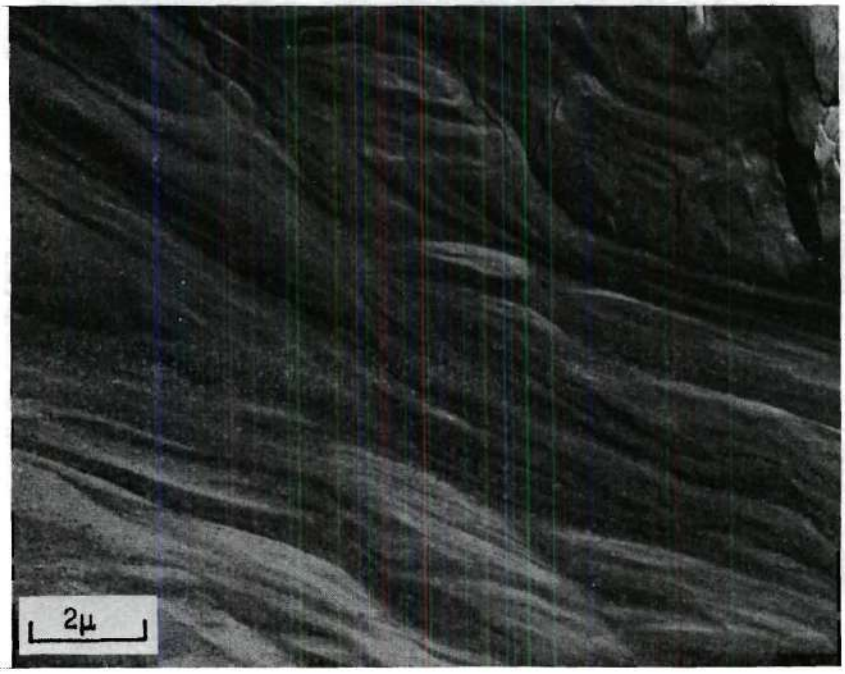

(b)

Figure 6. Electron Fractographs of the Ductile Areas of the Ti-2.5 Weight Percent Al Alloys, Laboratory-Air, Low-Hydrogen Failure: (a) Dimples, (b) Serpentine Glide

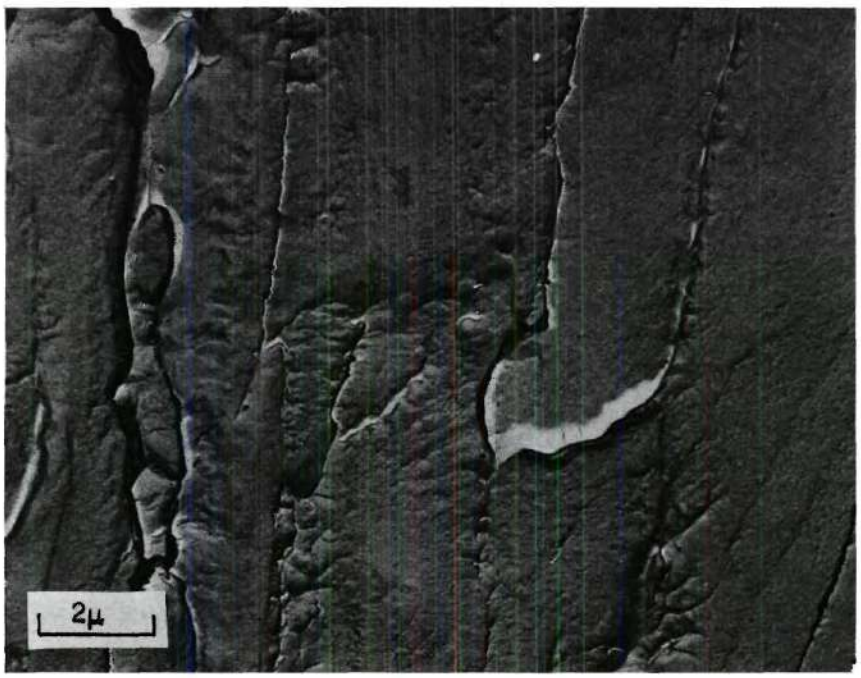

Figure 7. Electron Fractograph of the Flat Facet of the Ti-2.5 Weight Percent Al Alloy, Laboratory-Air, Low-Hydrogen Failure

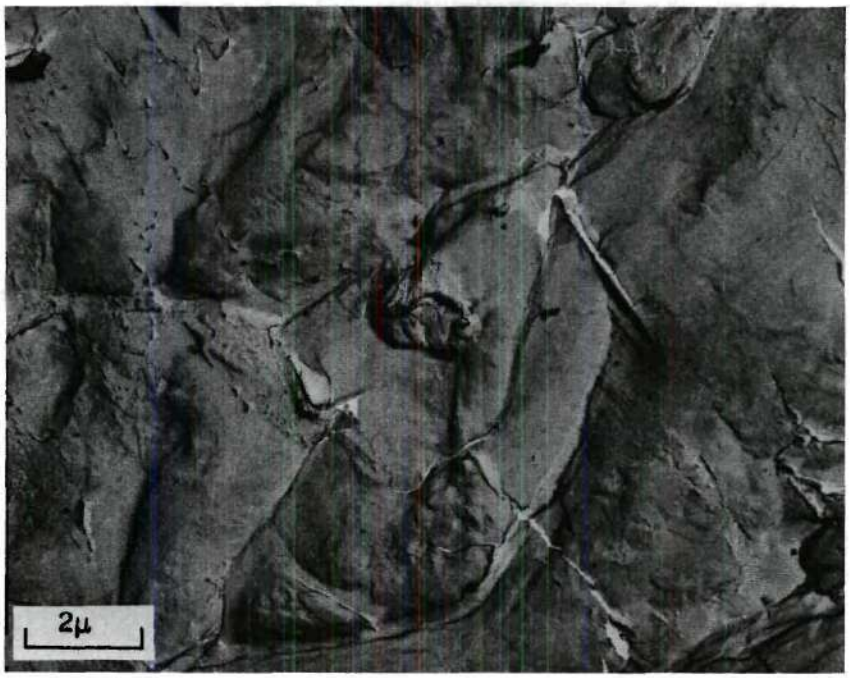

(a)

(b)

Figure 8. Electron Fractographs of a Ductile Area of the Ti-2.5 Weight Percent Al Alloy, 3.5 Percent NaCl Solution, Low-Hydrogen Failure: (a) Dimples, (b) Serpentine Glide

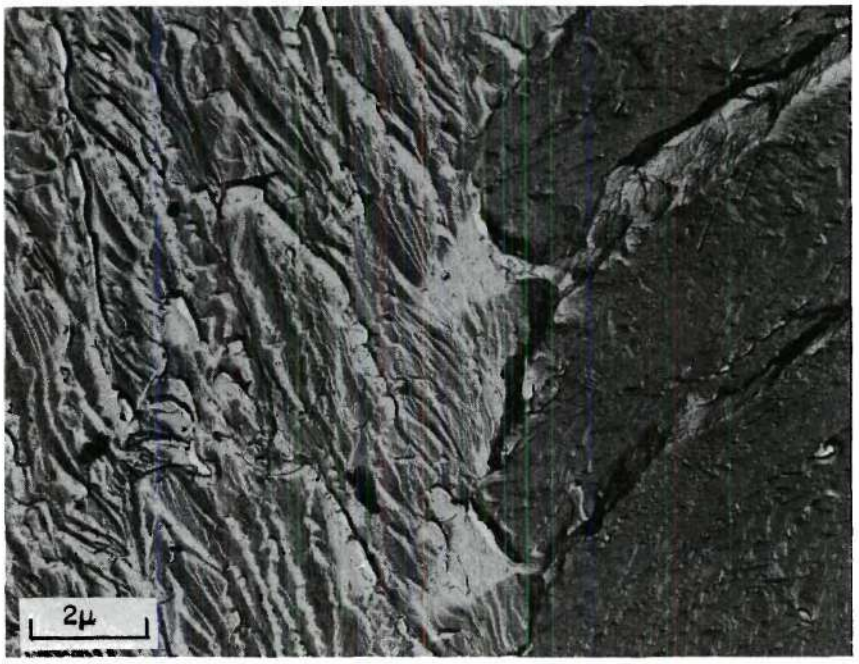

(a)

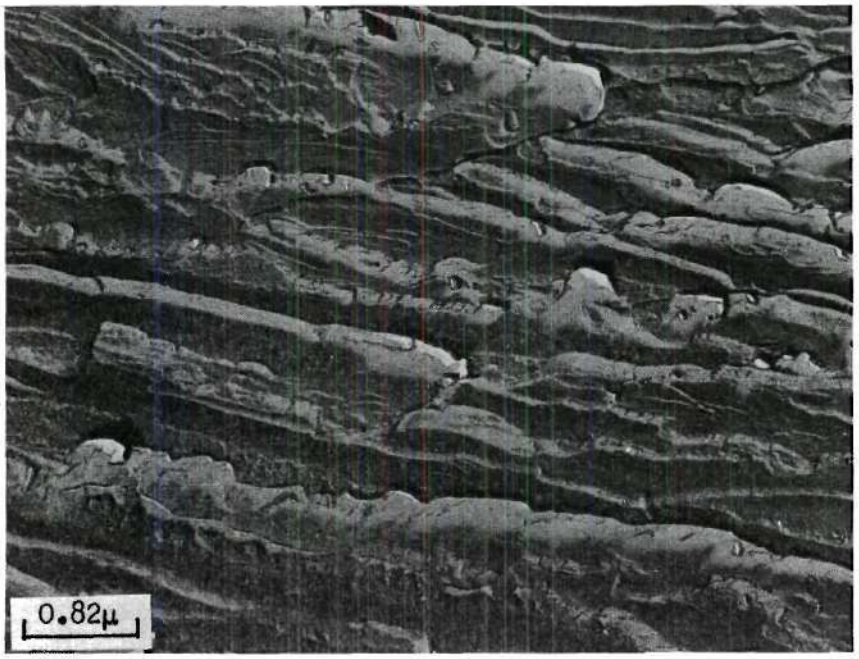

(b)

Figure 9. Electron Fractographs of the Flat Facets of the Ti-2.5 Weight Percent Al Alloy, Laboratory-Air, High-Hydrogen Failure: (a) Cleavage, (b) Cleavage

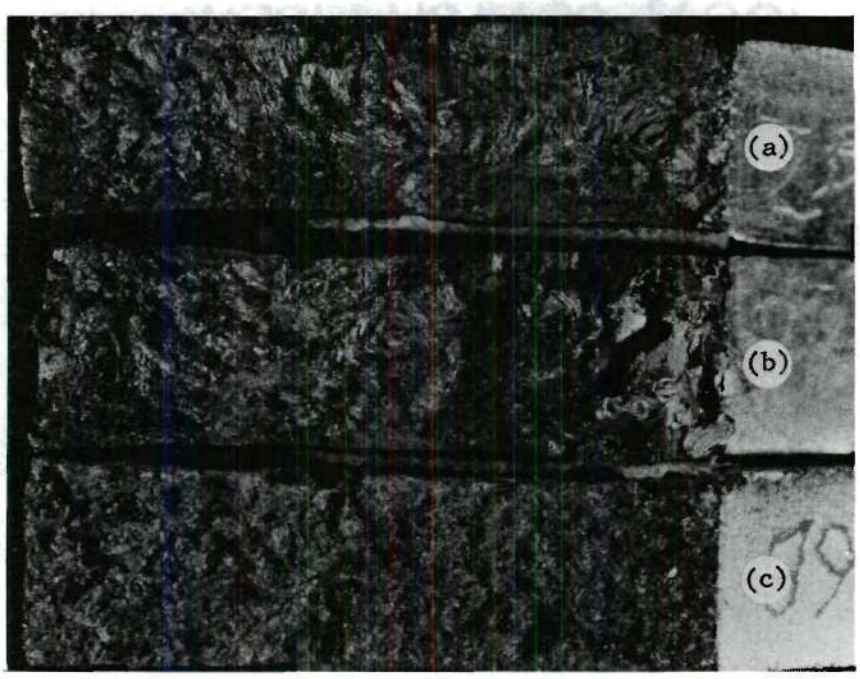

Figure 10. Light Macrographs of the Ti-5 Weight Percent Al Alloy Fracture Surfaces: (a) Laboratory-Air, Low-Hydrogen Failure, (b) 3.5 Percent NaCl Solution, Low-Hydrogen Failure, (c) Laboratory-Air, High-Hydrogen Failure (notch to right, crack propagation from right to left, magnification 4X)

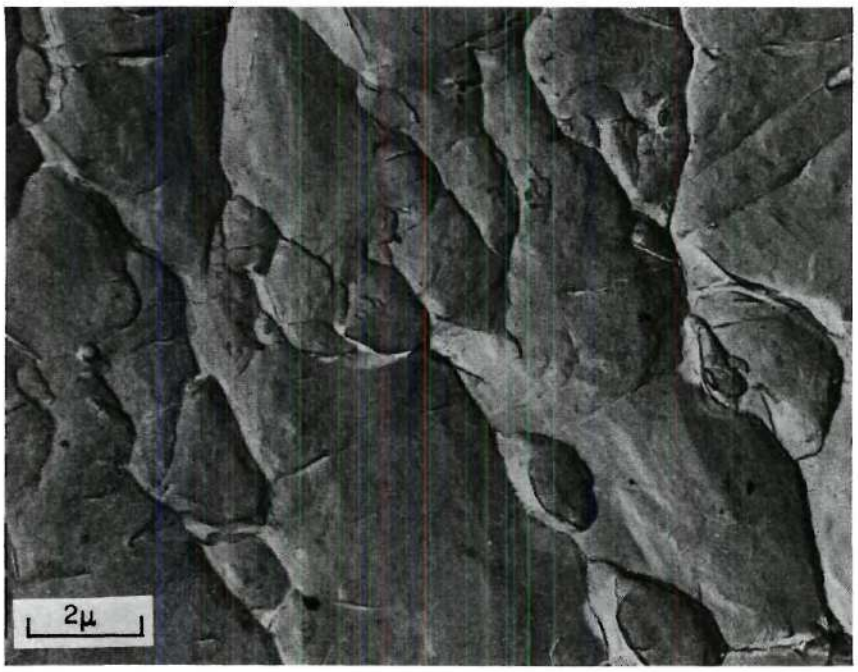

(a)

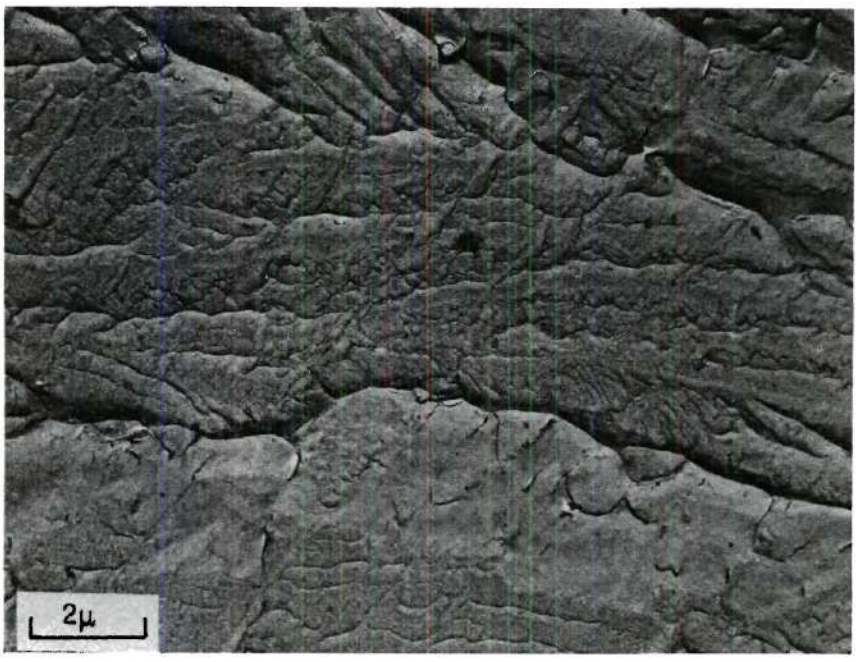

(b)

Figure 11. Electron Fractographs of the Ti-5 Weight Percent Al Alloy, Laboratory-Air, Low-Hydrogen Failure: (a) Dimples, (b) Dimples

showed flat facets near the notch, Figure 10b, and a ductile appearance at the opposite end. More specifically, fractographs of the flat facets showed a nonclassic type cleavage, Figure 12a, typical of SCC in Ti-Al alloys in the 5 to 6 weight percent range[60]. The ductile region was confirmed by the presence of dimples in Figure 12b. The high-hydrogen content specimen broken in laboratory air, contained smaller grains, as mentioned previously. The fracture surface of this specimen was characterized by a mixture of ductile and faceted areas adjacent to the notch and an all ductile region at the opposite end, Figure 10c. All ductile regions were confirmed by the appearance of dimples in the fractographs, Figure 13a. The near-classic-cleavage appearance of the flat facets, Figure 13b, confirmed SSRHE of this specimen.

Ti-8 Weight Percent Al Alloy. The low-hydrogen content specimen of the Ti-8 weight percent Al alloy, failed in laboratory air, had a fracture surface containing both flat facets and ductile appearing regions, Figure 14a. The ductile areas were characterized by serpentine glide, Figure 15a, and the flat facets by nonclassic cleavage, Figure 15b, similar to that previously observed[61] for nonenvironmental failures of Ti-8 weight percent Al alloys. The 3.5 percent NaCl solution failure showed all flat facets near the notch and a mixture of these facets and ductile areas on the opposite end, Figure 14b. Figure 16a was typical of the ductile areas and Figure 16b was typical of the nonclassic cleavage seen in SCC of Ti-8 weight percent Al alloys[61]. The whole fracture surface of the laboratory-air, high-hydrogen content sample contained flat facets, except for a few small ductile areas to the extreme left, Figure 14c. The nonclassic cleavage shown in Figure

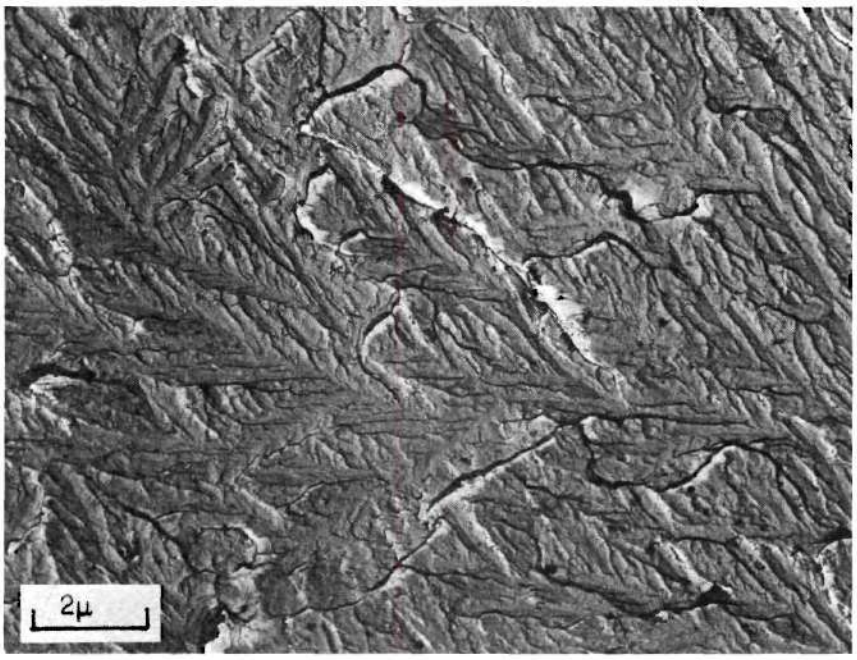

(a)

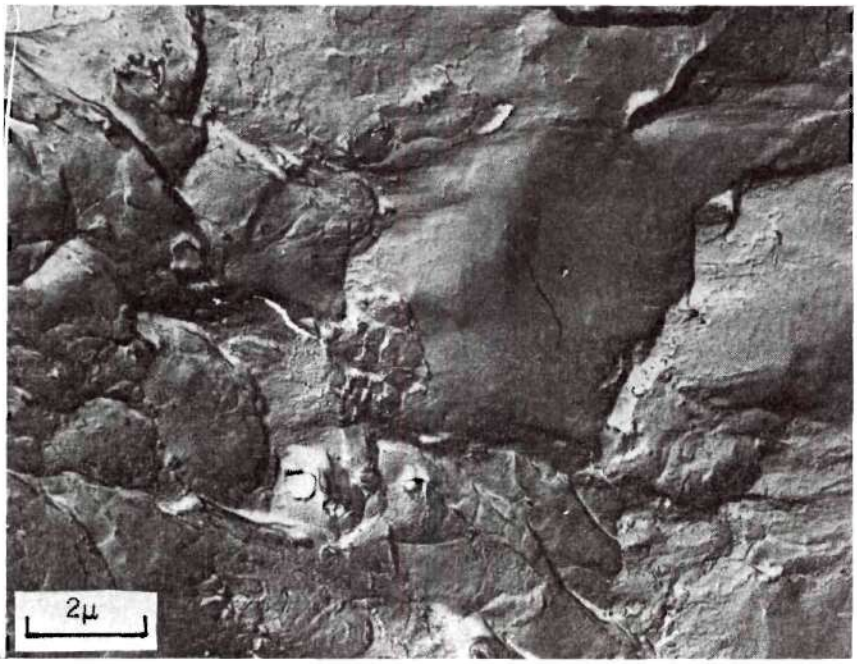

(b)

Figure 12. Electron Fractographs of the Ti-5 Weight Percent Al Alloy, 3.5 Percent NaCl Solution, Low-Hydrogen Failure: (a) Nonclassic Cleavage, (b) Dimples

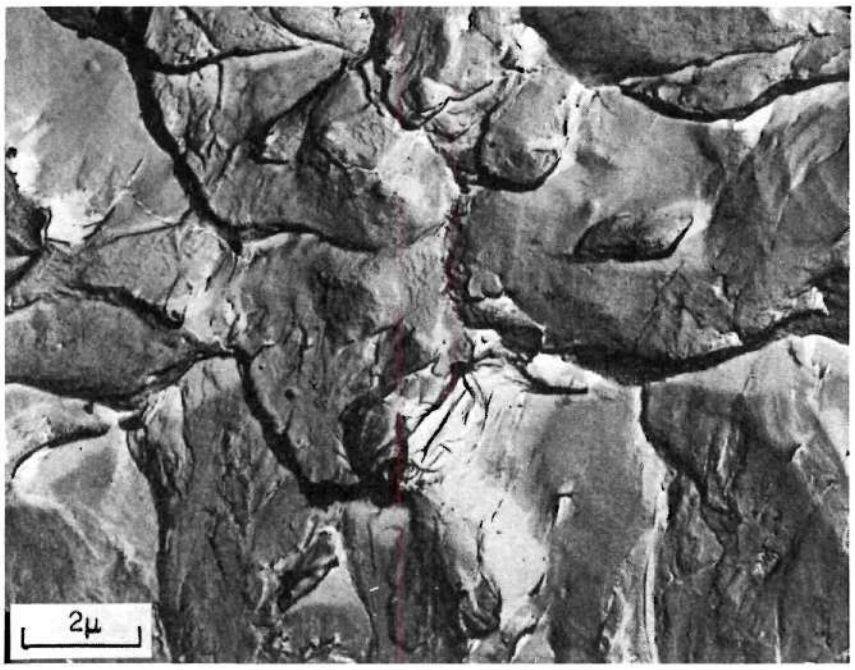

(a)

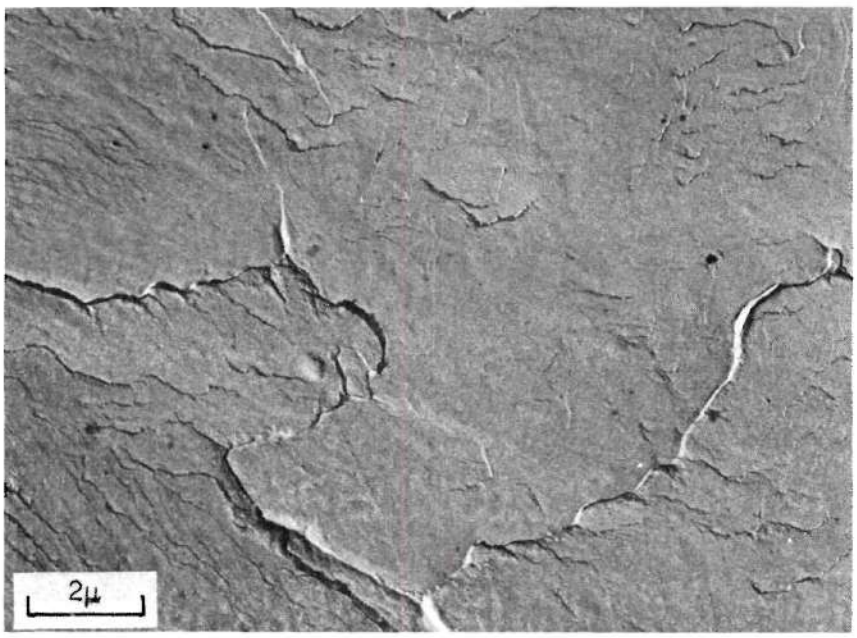

(b)

Figure 13. Electron Fractographs of the Ti-5 Weight Percent Al Alloy, Laboratory-Air, High-Hydrogen Failure: (a) Dimples, (b) Near-Classic Cleavage

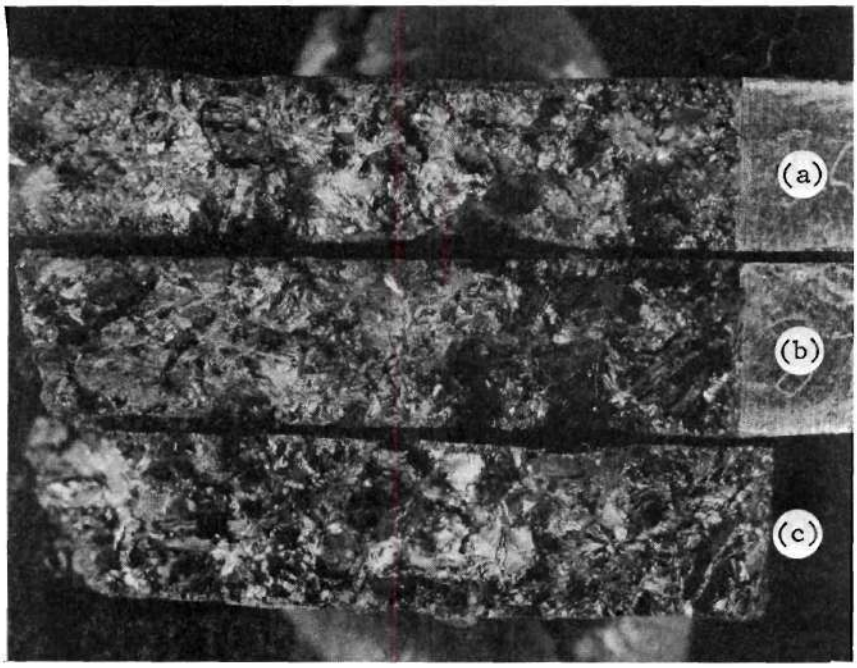

Figure 14. Light Macrographs of the Ti-8 Weight Percent Al Alloy Fracture Surfaces: (a) Laboratory-Air, Low-Hydrogen Failure, (b) 3.5 Percent NaCl Solution, Low-Hydrogen Failure, (c) Laboratory-Air, High-Hydrogen Failure (notch at right, crack propagation from right to left, magnification 4X)

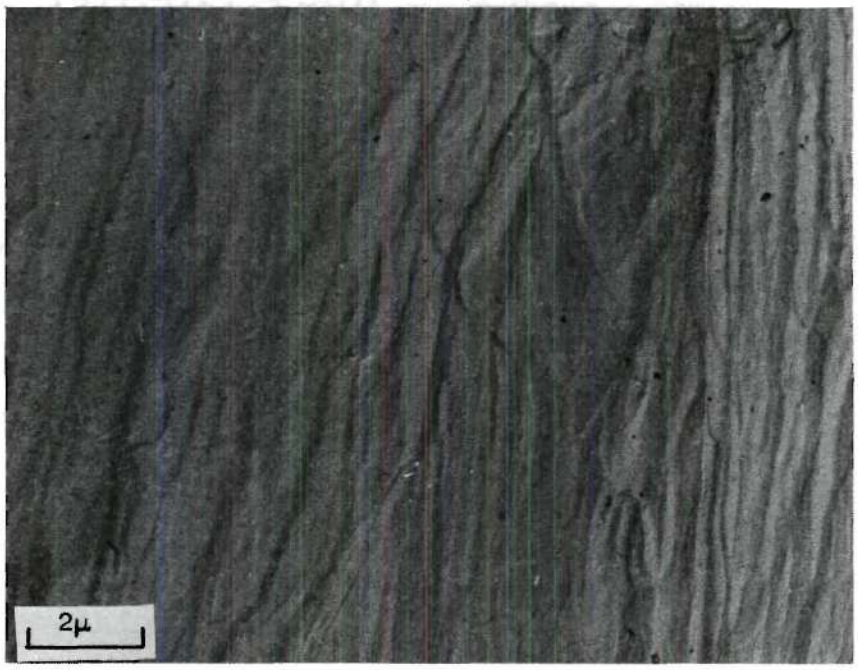

(a)

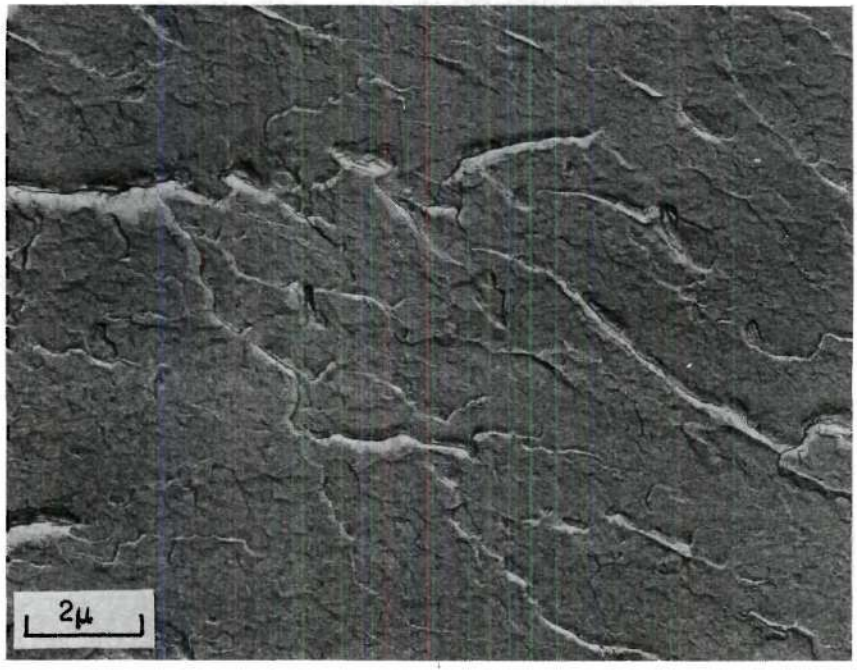

(b)

Figure 15. Electron Fractographs of the Ti-8 Weight Percent Al Alloy, Laboratory-Air, Low-Hydrogen Failure: (a) Serpentine Glide, (b) Nonclassic Cleavage

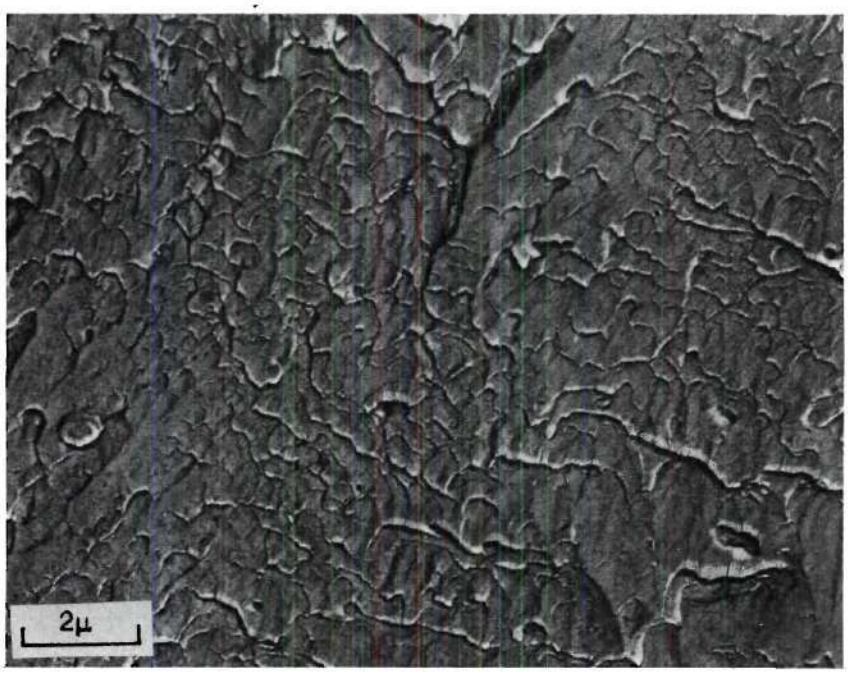

(a)

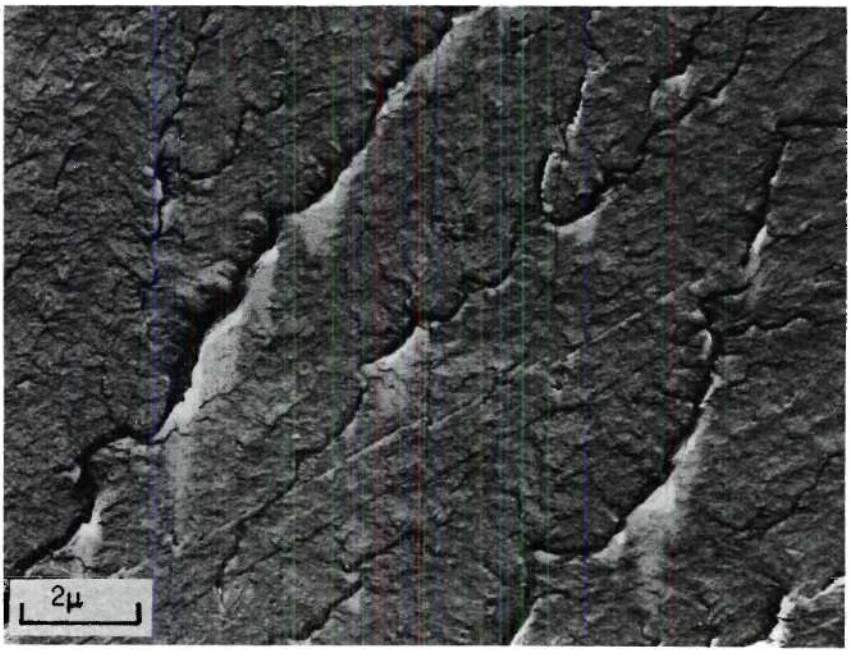

(b)

Figure 16. Electron Fractographs of the Ti-8 Weight Percent Al Alloy, 3.5 Percent NaCl Solution, Low-Hydrogen Failure: (a) Dimples, (b) Nonclassic Cleavage

17a was typical of the flat facets indicating SSRHE, and the serpentine glide shown in Figure 17b was typical of the small ductile areas.

Fracture Habit Plane

Orientation determinations of the fracture planes were attempted on suitable facets using the Laue technique described in Chapter II. The facets on the Ti-2.5 weight percent Al, laboratory-air, high-hydrogen content sample were unsuitable due to their small size, as were all but one on the Ti-5 weight percent Al, laboratory-air, high-hydrogen content sample. The poles of the fracture planes which were determined are plotted in a (0001) polar stereographic projection, by both Al content, Figure 18a, and fracture environment and hydrogen content, Figure 18b. All fracture planes determined were found to be oriented within 15^{o} of the basal plane.

Deformation Mode as Characterized by Transmission Electron Microscopy

Slip was the only deformation mode observed in the present investigation. The Ti-2.5 weight percent Al samples showed dislocation tangles typical of this alloy[4] in both the low- and high-hydrogen content specimens, Figure 19a and 19b. The Ti-5 weight percent Al alloy specimens showed coplanar arrays in the low-hydrogen content specimen, Figure 20a, and coplanar arrays containing hydrides in the high-hydrogen content specimen, Figure 20b. Coplanar arrays of dislocations were seen in both the low- and high-hydrogen content, Ti-8 weight percent Al alloy specimens, Figure 21a and 21b, respectively. No hydrides were observed in either specimen.

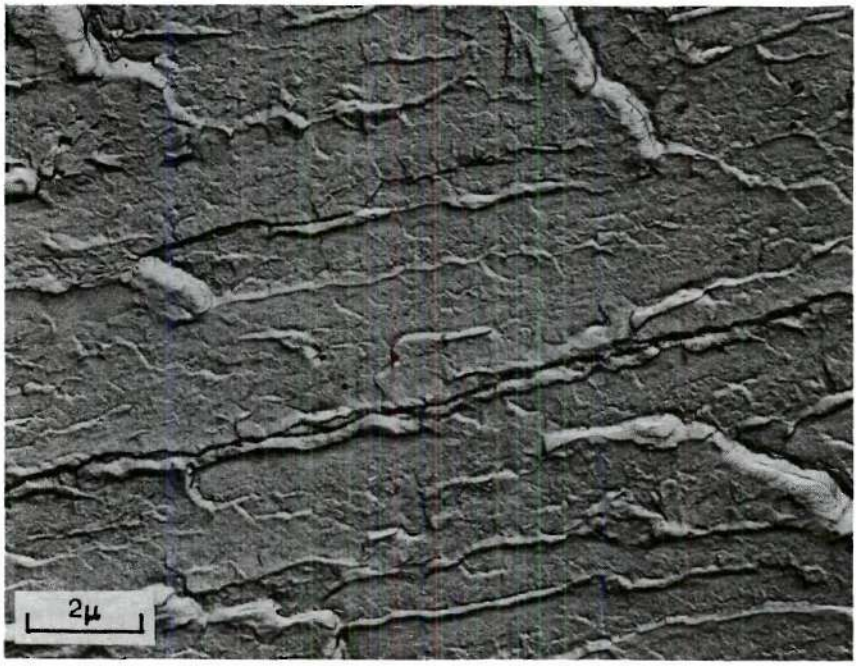

(a)

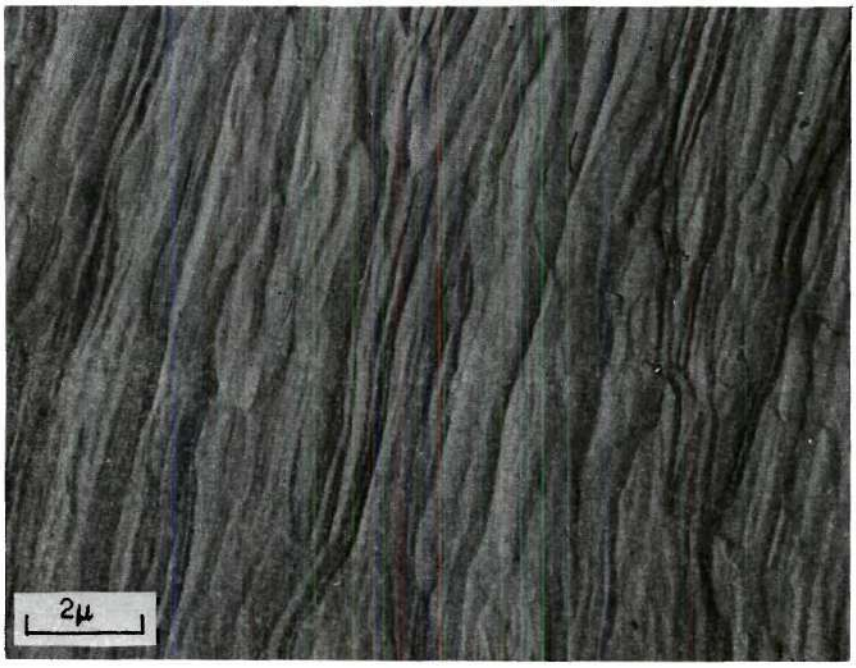

(b)

Figure 17. Electron Fractographs of the Ti-8 Weight Percent Al Alloy, Laboratory-Air, High-Hydrogen Failure: (a) Nonclassic Cleavage, (b) Serpentine Glide

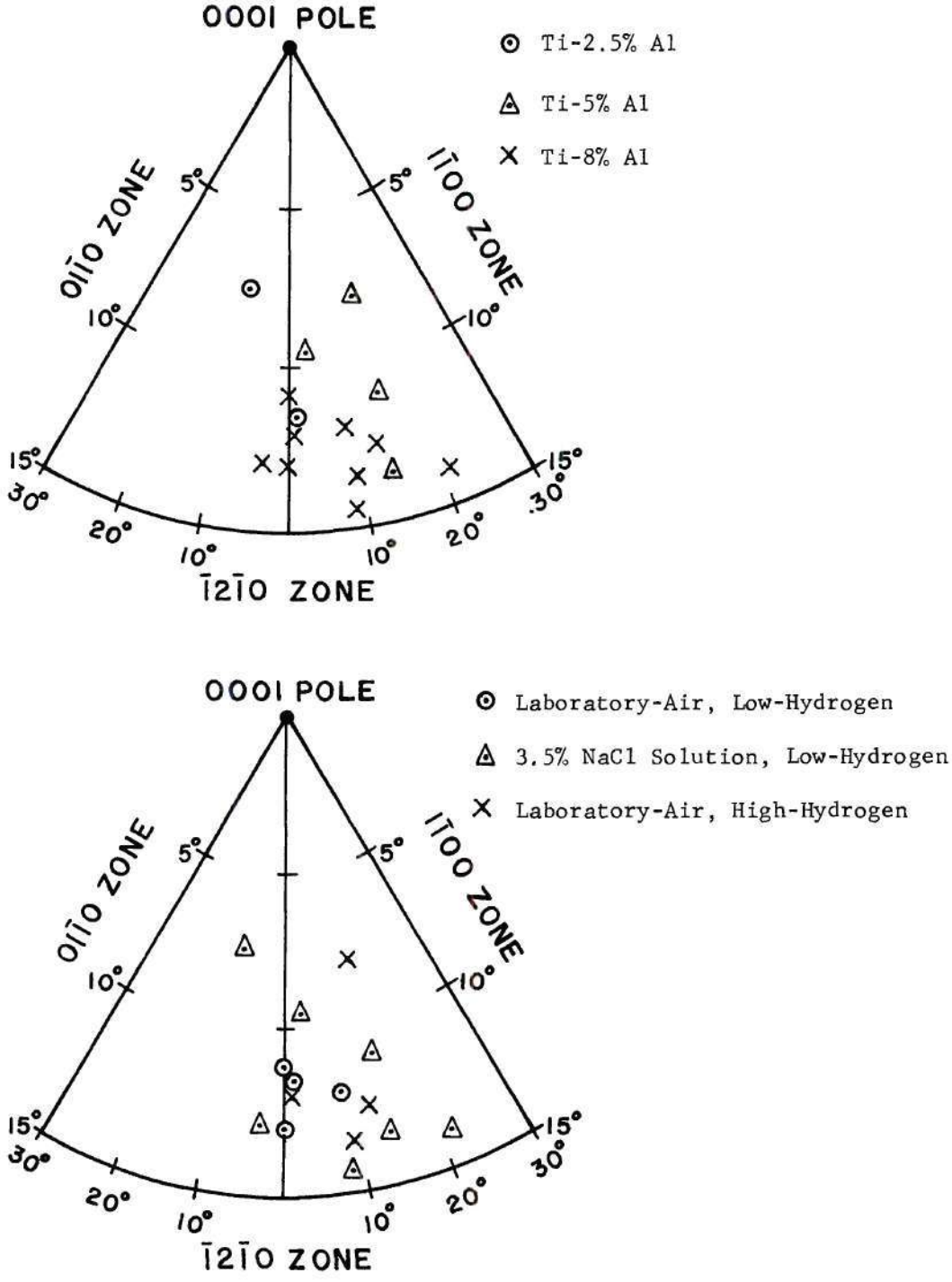

Figure 18. (0001) Polar Stereographic Projections Showing the Relative Orientations of the Fracture Facets: (a) Plotted by Al Content, (b) Plotted by Fracture Environment and Hydrogen Content

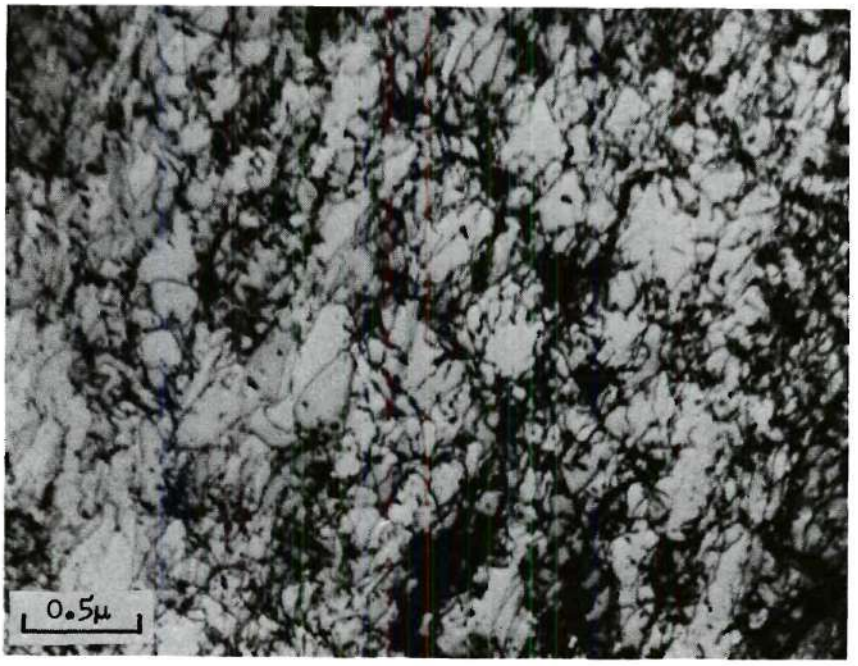

(a)

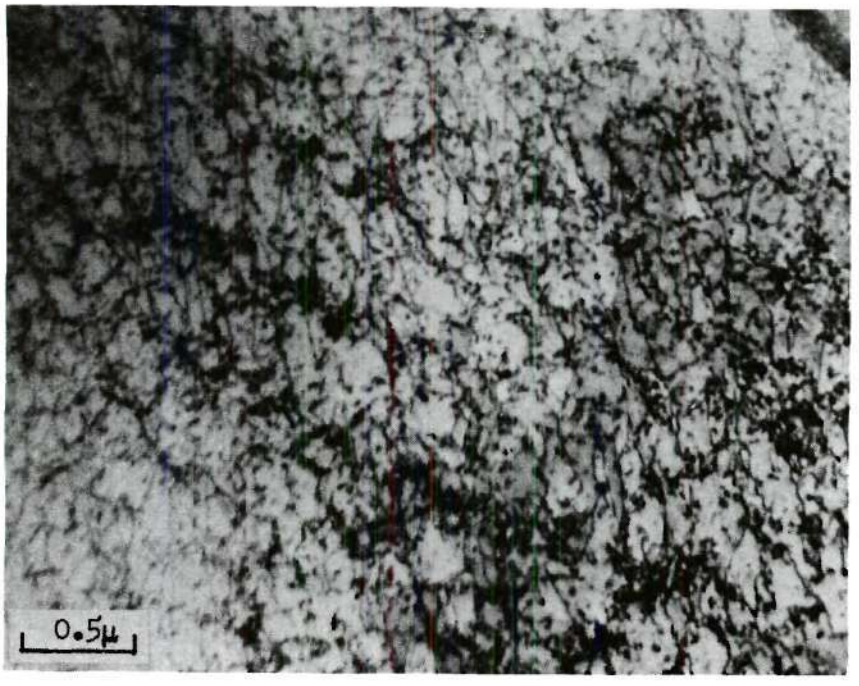

(b)

Figure 19. Transmission Electron Micrographs of Strained Ti-2.5 Weight Percent Al Alloy: (a) Dislocation Tangles in Low-Hydrogen Alloy, (b) Dislocation Tangles in High-Hydrogen Alloy

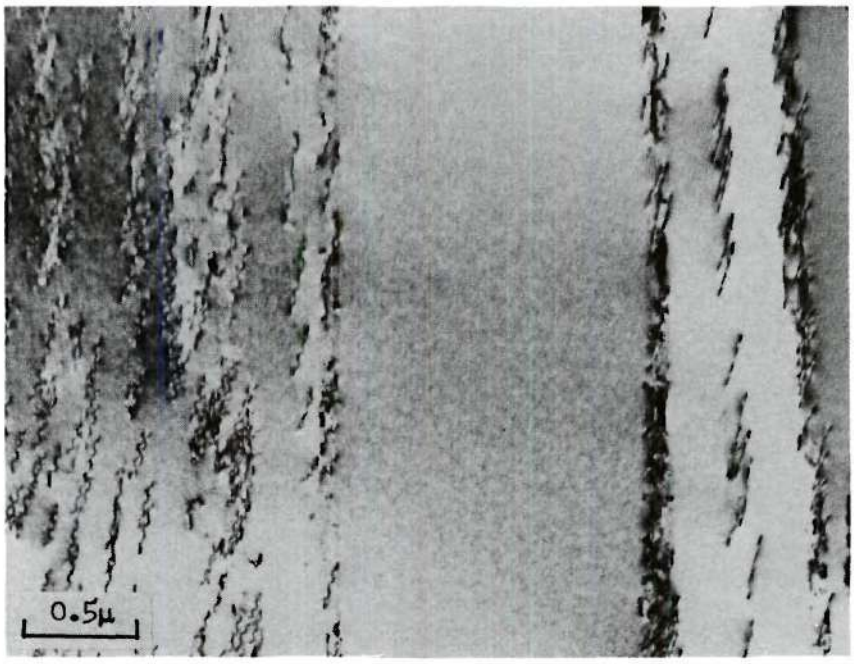

(a)

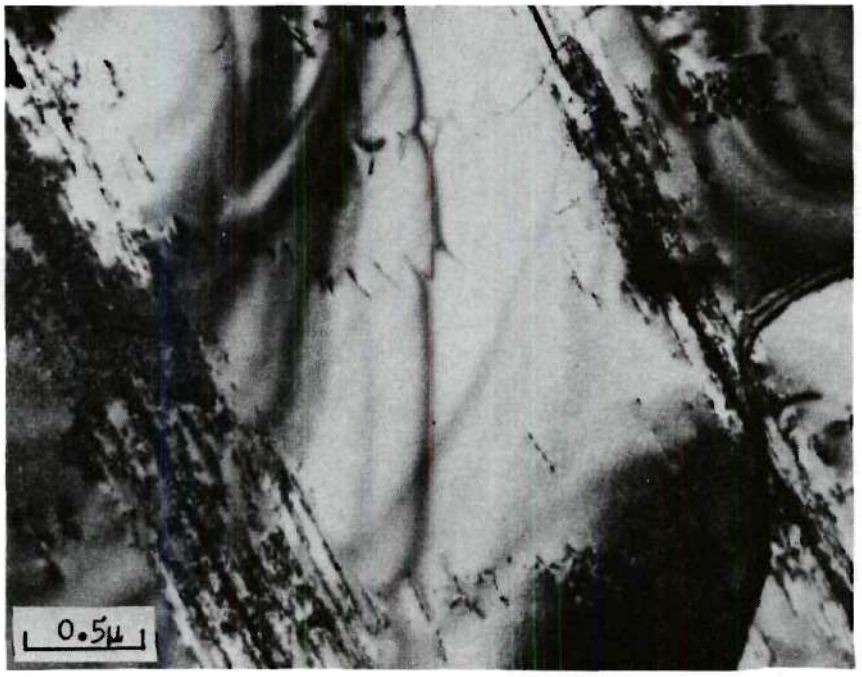

(b)

Figure 20. Transmission Electron Micrographs of Strained Ti-5 Weight Percent Al Alloy: (a) Dislocation Coplanar Arrays in Low-Hydrogen Alloy, (b) Ti-Hydrides Precipitated in Dislocation Coplanar Arrays in High-Hydrogen Alloy

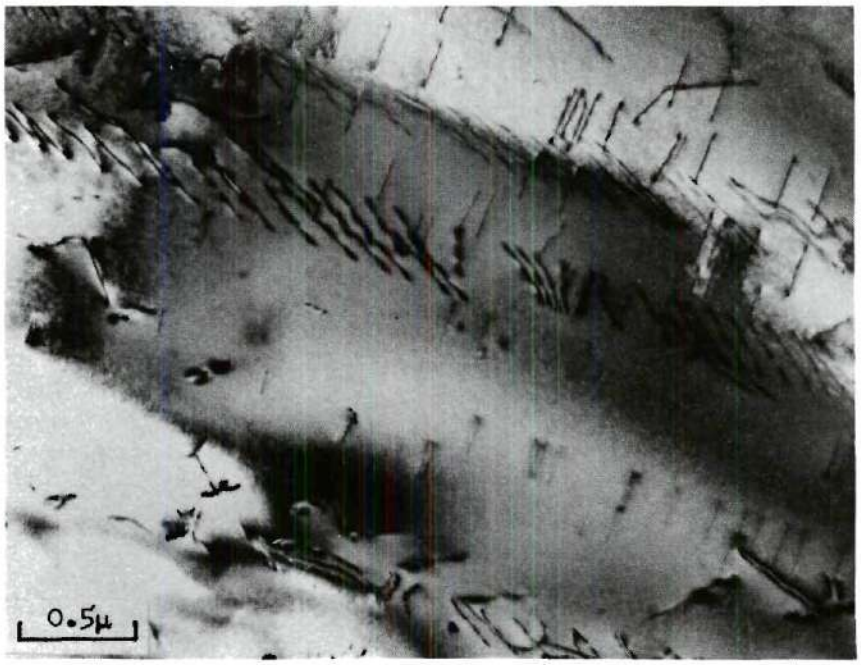

(a)

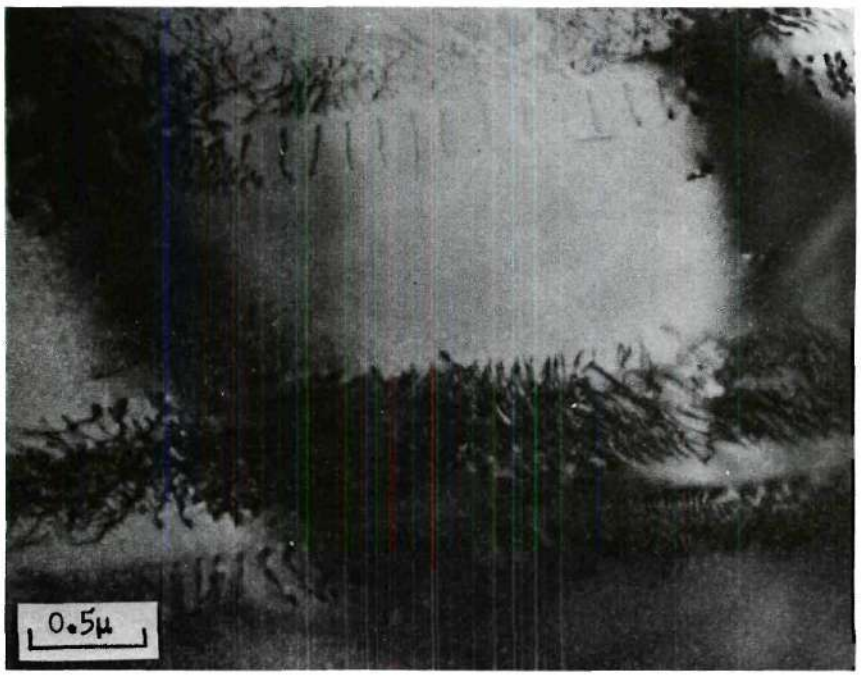

(b)

Figure 21. Transmission Electron Micrographs of Strained Ti-8 Weight Percent Al Alloy: (a) Dislocation Coplanar Arrays in Low-Hydrogen Content Alloy, (b) Dislocation Coplanar Arrays in High-Hydrogen Content Alloy

CHAPTER IV

DISCUSSION OF RESULTS

The results of the present study support the suggestion by Mukherjee[1] that there is a correlation between the fracture modes of SCC and SSRHE in Ti-Al alloys. Similar decreases in K_{Ix} during SCC and SSRHE of the 5 and 8 weight percent Al samples, along with comparative fracture characteristics, are the basis for this conclusion.

The Ti-2.5 weight percent Al alloy was not susceptible to SCC which substantiates the results of Blackburn and Williams[4]. The insignificant change observed in K_{Ix} during SSRHE and the similarity between the deformation characteristics of the low- and high-hydrogen content specimens offers no indication of the mechanism for SSRHE for this alloy.

The significant results of the present study were concerned with the Ti-5 and 8 weight percent Al alloys. There was a definite similarity between SCC failure and the SSRHE failure of the Ti-5 weight percent Al alloy. Both failures were accompanied by a decrease of the K_{Ix} values and both were characterized by cleavage near the notched areas. The precipitation of hydrides in the slip bands of the high-hydrogen content specimen, and not in the low-hydrogen content specimen, lends support to the suggestion by Boyd[30] made for Ti-8-1-1, that hydrogen plays a role in SCC. The difference in the appearance of the electron fractographs of the cleavage facets of the SCC fracture and the SSRHE fracture is not absolutely clear. It is possible, however, that this discrepancy

is due to hydrogen having to diffuse into the sample from the surface reaction during the SCC process, whereas it is already present in the matrix of the sample undergoing SSRHE.

Further support for hydrogen contributing to both SCC and SSRHE is obtained by closely examining the results of the Ti-8 weight percent Al alloy. There was a similar decrease of the K_{Ix}, or load values, for both SCC and SSRHE samples. In addition, nonclassic cleavage was observed near the notch regions in both cases. The laboratory-air failure of the low-hydrogen content specimens also contained nonclassic cleavage, but in this case it was mixed with ductile areas. The nonclassic cleavage seems to be a characteristic of Ti-8 weight percent Al alloys.

Although hydrides were not observed on the slip bands of the high-hydrogen content, Ti-8 weight percent Al alloy in the area examined, this does not eliminate the possibility of their existence in the fracture region. The strain obtained in the area of examination, which was somewhat removed from the actual failure region, was probably insufficient to stimulate hydride precipitation.

The difference between the appearance of the cleavage in fractographs of the 5 and 8 weight percent Al alloys must also be considered. One explanation for these differences might be the presence of short-range order in the Ti-5 weight percent Al alloy[19], whereas long-range order domains are present in the Ti-8 weight percent Al alloy. The presence of these domains was confirmed by electron diffraction patterns which clearly showed supperlattice reflections, Figure 22.

Figure 18a and 18b show that the orientation of all of the facets examined were within 15° of the basal plane. The scatter of the data

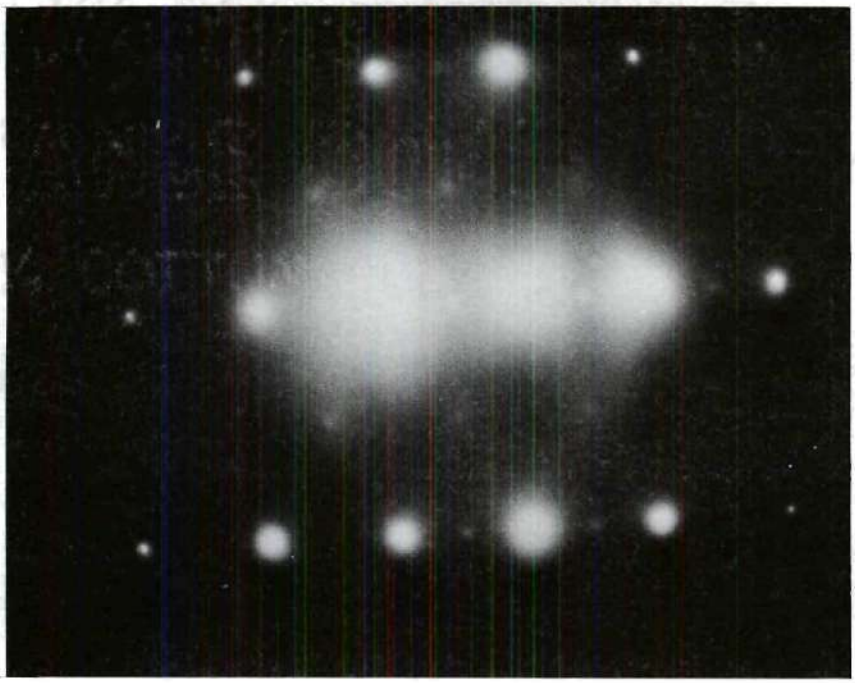

Figure 22. Electron Diffraction Pattern of the Ti-8 Weight Percent Al, Low-Hydrogen Content Specimen Showing Fundamental and Superlattice Reflections ([$2\bar{1}\bar{1}6$] Zone Normal)

prevented definite indices being assigned to the fracture plane; however, the fact that all possessed approximately the same orientation is quite significant. This strongly suggests that a plane close to the basal plane is the normal cleavage plane for Ti-Al binary alloys.

Various slip steps were observed on the Ti-8 weight percent Al alloy, SCC replicas. Since slip occurs predominately on $\{10\bar{1}0\}$ and $\{10\bar{1}1\}$, this suggests a means for confirming or eliminating the possibility of the observed fracture plane being a combination of basal and nonbasal cleavage. A series of fractographs was taken from different replica tilts and it was assumed that when the distance between slip steps was maximized the replica was perpendicular to the electron beam[62]. The slip steps, indicated by arrows in Figure 23, would intersect the cleavage facets forming equilateral triangles if the facets were parallel to the basal plane. Typical angular measurements from these triangles were 59°, 65°, 56°, suggesting that these facets were close to, but not parallel to the basal plane, in agreement with the X-ray results.

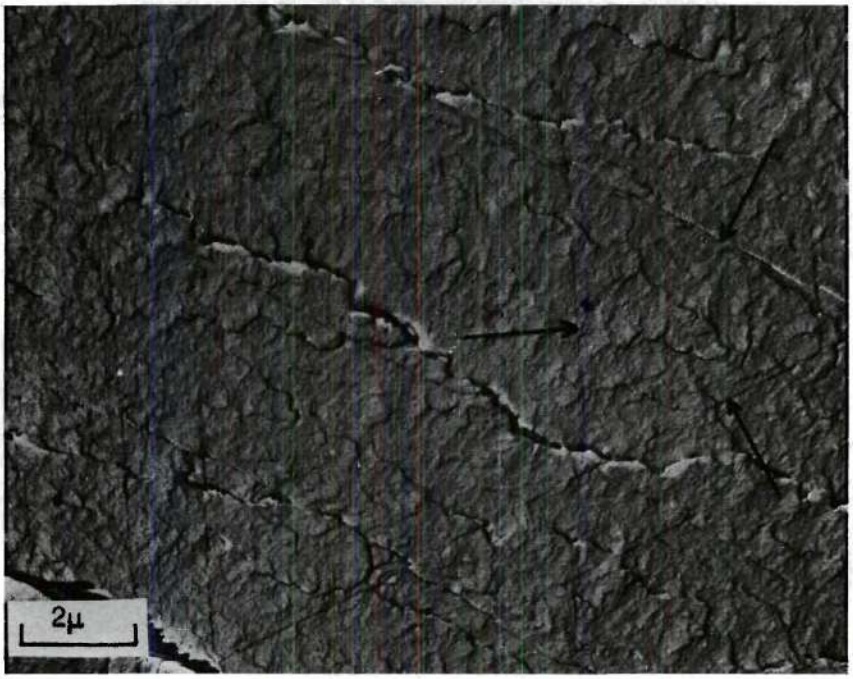

Figure 23. Electron Fractograph of the Ti-8 Weight Percent Al, 3.5 Percent NaCl Solution, Low-Hydrogen Fracture Surface Showing Triangles Formed by Slip Steps (indicated by arrows)

CHAPTER V

CONCLUSIONS

1. The similarities between observed SCC and SSRHE failures in Ti-5 and 8 weight percent Al alloys strongly suggest that hydrogen plays a significant role in the SCC process.

2. Although the definite role of hydrogen was not determined, the present observations indicate that the precipitation of hydrides on coplanar dislocations is related to the mode of SCC and SSRHE failure in Ti-Al alloys.

3. The cleavage habit plane observed for SCC, which is close to but not the basal plane, appears to be the prominent fracture plane for all brittle failures of these Ti-Al binary alloys.

APPENDIX

HIGH-TEMPERATURE-INERT-ATMOSPHERE-QUENCH FURNACE

As described in Chapter II, homogenization at 1400°C was required to remove the Al partitioning resulting from hot rolling in the $\alpha+\beta$ phase field and to allow β grain coarsening, which results in large α martensite needles on cooling. Quenching from this temperature prevents partitioning from occurring by not dwelling in the $\alpha+\beta$ phase field[49]. Due to titanium's high affinity for oxygen[5], this homogenization and β-quench must be performed in an inert atmosphere.

A high-temperature-inert-atmosphere-quench furnace was built to carry out this operation. The outer surface of the furnace body (1) (numbers in parenthesis correspond to numbers in Figure 24) was insulated with 2 inches of Monoblock (mineral wool block) and the inner surface with 5 inches of Alundum 33-I (castable alumina insulation). Inside was a hollow open end cylindrical heating element of Crusilite (silicon carbide) with an inside diameter of 2.64 inches and 11.8 inches long hot zone. Inside this heating element was a 28-inch long zirconium ceramic tube with a 2-inch inside diameter. To each end of this tube was welded a 30-inch extension of Pyrex glass tubing with a 2-inch inside diameter. These welds were cooled by cooling the air around them with water flowing through copper coils (2). Over the top of the tube was placed a cap (3) where double-liquid-nitrogen-trapped (4) ultra-high-purity helium (99.999 percent minimum purity excluding neon) (5)

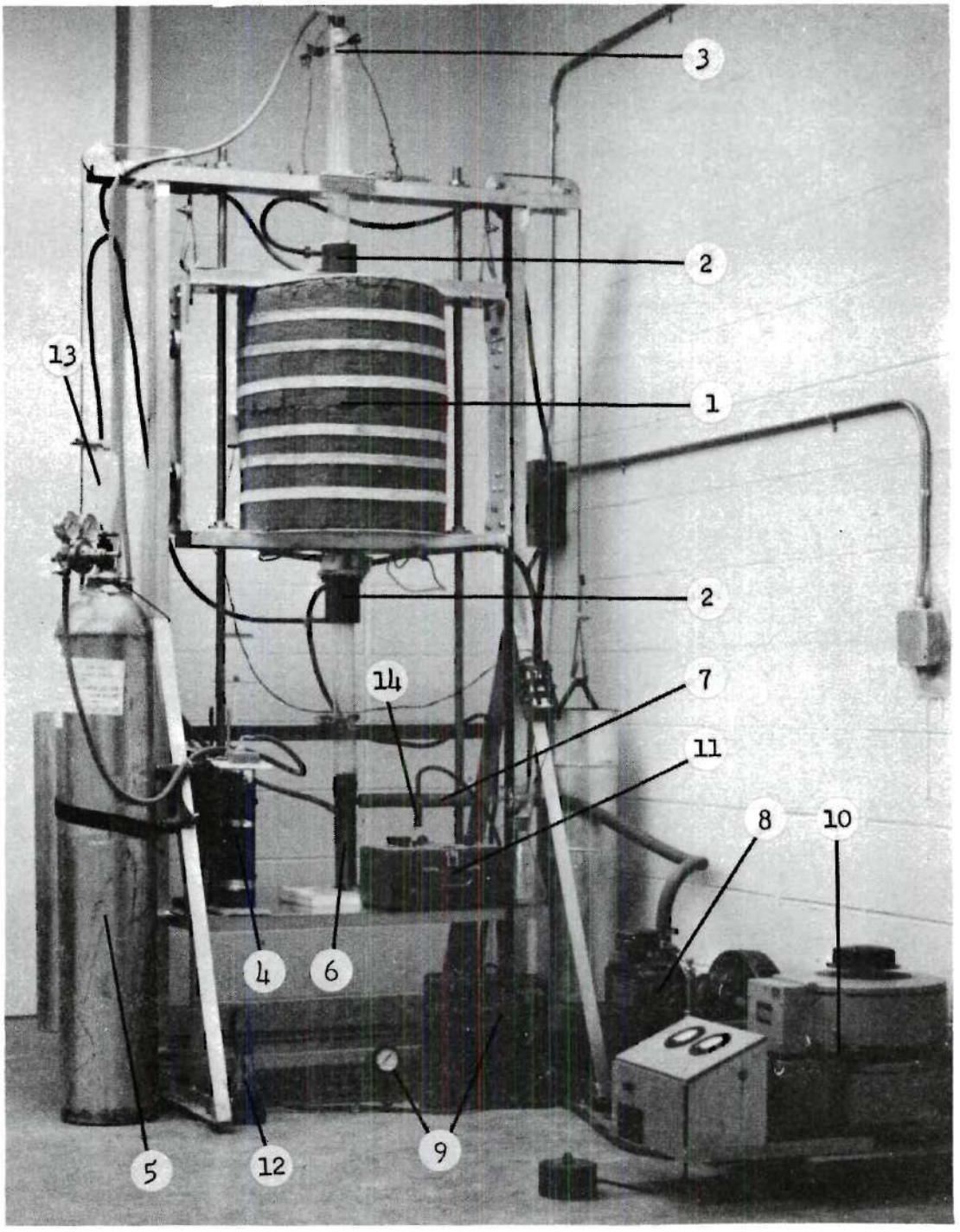

Figure 24. High-Temperature-Inert-Atmosphere-Quench Furnace (numbers correspond to numbers in text)

was passed into the tube. A copper quench cup (6) was sealed to the bottom of the tube by jeweler's wax from which a vacuum line (7) ran to a rotary vacuum pump (8) for evacuating the tube. A Stoke's McLeod gauge and vacuum dial gauge (9) were used to monitor the pressure in the tube. The temperature was controlled by the output from a General Electric volt-pac variable transformer (10) and monitored by a Leeds and Northrup potentiometer (11) connected to a Pt/Pt-13 weight percent Rh thermocouple.

The specimen to be heat-treated was held in the top of the tube by a tungsten wire clamped to the cap (3). The tube was then evacuated by the rotary pump (8) to a pressure of approximately 0.3 torr. Next, ultra-high-purity helium was let in until a pressure of one atmosphere was reached. This purging process was repeated three times and then, with a small positive pressure, helium was slowly bubbled through oil at the exit tube (12). Without air entering, the specimen was slowly lowered by the tungsten support wire to the center of the furnace body where the temperature was at 1400 ± 20°C over a 7-inch long zone. After 6 hours 55°C water from the reservoir (13) was let into the quench cup (6). The specimen was then released by the clamp in the tube cap (3) and quenched in the water. The resulting steam pressure was relieved by a blow-out plug (14). The specimen was removed from the quench cup by melting the jeweler's wax around it and removing the cup.

BIBLIOGRAPHY*

1. A. K. Mukherjee, "The Possible Role of Hydrogen in Stress Corrosion Cracking of Titanium Alloys," Boeing Company Document D6-23621, Renton, Washington, September, 1967.

2. B. F. Brown, "A New Stress-Corrosion Cracking Test for High-Strength Alloys," Materials Research and Standards, Vol. 6, 1966, p. 129.

3. D. N. Fager and W. F. Spurr, "Some Characteristics of Aqueous Stress-Corrosion in Titanium Alloys," Trans. Am. Soc. Metals, Vol. 61, 1968, p. 283.

4. M. J. Blackburn and J. C. Williams, "Metallurgical Aspects of Stress Corrosion Cracking of Titanium Alloys," Paper presented at the Conference on the Fundamental Aspects of Stress Corrosion Cracking, Columbus, Ohio, September, 1967.

5. H. Margolin and J. P. Nielsen, "Titanium Metallurgy," Modern Materials; Advances in Development and Applications, Vol. 2, 1960, p. 225.

6. R. I. Jaffee, "The Physical Metallurgy of Titanium Alloys," Progress in Metal Physics, Vol. 7, 1958, p. 65.

7. H. R. Ogden, D. J. Maykuth, W. L. Finlay, and R. I. Jaffee, "Constitution of Titanium-Aluminum Alloys," Trans. TMS-AIME, Vol. 191, 1951, p. 1150.

8. E. S. Bumps, H. D. Kessler, and M. Hansen, "Titanium-Aluminum System," Trans. TMS-AIME, Vol. 194, 1952, p. 609.

9. K. Sagel, E. Schulz, and U. Zwicker, "Studies of the Titanium-Aluminum System," Z. Metallk., Vol. 47, 1956, p. 529.

10. K. Anderko, K.Sagel, and U. Zwicker, "Hexagonal Ordered Phases in the Systems Titanium-Aluminum (Titanium-Aluminum-Indium) and Titanium-Indium," Z. Metallk., Vol. 48, 1957, p. 57.

---

* Abbreviations found herein follow the form used by Transactions of the Metallurgical Society of the American Institute of Mining, Metallurgical, and Petroleum Engineers, Vol. 239, 1967, p. 1200.

11. F. A. Crossley and W. F. Carew, "Embrittlement of Ti-Al Alloys in the 6 to 10 % Al Range," Trans. TMS-AIME, Vol. 209, 1957, p. 43.

12. E. Ence and H. Margolin, "Compounds in the Titanium-Rich Region of the Ti-Al System," J. Metals, Vol. 9, 1957, p. 484.

13. J. Schroeder, "Investigation of the Ordered Phase Ti_3Al," M.S. Thesis, Ohio State University, 1958.

14. H. R. Ogden, D. J. Maykuth, W. L. Finlay, and R. I. Jaffee, "Mechanical Properties of High Purity Ti-Al Alloys," Trans. TMS-AIME, Vol. 197, 1953, p. 267.

15. M. K. McQuillan, "Phase Transformations in Titanium and Its Alloys," Metallurgical Reviews, Vol. 8, 1963, p. 41.

16. M. J. Blackburn, "Phase Transformations in the Alloy Ti-8Al-1Mo-V," Trans. Am. Soc. Metals, Vol. 59, 1966, p. 876.

17. J. B. Newkirk, A. H. Geisler, "Crystallographic Aspects of the Beta to Alpha Transformation in Titanium," Acta Met., Vol. 1, 1953, p. 370.

18. C. J. McHargue, "The Crystallography of the Titanium Transformation," Acta Crystallographica, Vol. 6, 1953, p. 529.

19. M. J. Blackburn, "The Ordering Transformation in Titanium:Aluminum Alloys Containing Up to 25 At. Pct. Aluminum," Trans. TMS-AIME, Vol. 239, 1967, p. 1200.

20. F. A. Crossley, "Titanium-Rich End of the Ti-Al Equilibrium Diagram," Trans. TMS-AIME, Vol. 236, 1966, p. 1174.

21. H. Margolin, "Discussion of 'The Ordering Transformation in Titanium:Aluminum Alloys Containing Up to 25 At. Pct. Aluminum'," Trans. TMS-AIME, Vol. 242, 1968, p. 742.

22. H. Margolin and H. Portisch, "Hydrogen-Induced Expansions in Titanium-Aluminum Alloys," Trans. TMS-AIME, Vol. 242, 1968, p. 1901.

23. T. Tsujimoto and M. Adachi, "Reinvestigation of the Titanium-Rich Region of the Titanium-Aluminum Equilibrium Diagram," J. Inst. Metals, Vol. 94, 1966, p. 358.

24. T. Sato, Y. C. Huang, and Y. Kondo, "Equilibrium Diagram of the System Ti-Al," J. Japan Inst. of Metals, Vol. 53, 1959, p. 456.

25. D. Clark, K. S. Jepson, and G. I. Lewis, "A Study of the Titanium-Aluminum System Up to 40 At. -% Aluminum," J. Inst. Metals, Vol. 91, 1963, p. 197.

26. P. Cotterill, "The Hydrogen Embrittlement of Metals," Progress in Material Science, Vol. 9, 1961, p. 201.

27. A. D. McQuillan, "An Experimental and Thermodynamic Investigation of the Hydrogen-Titanium System," Proc. Roy. Soc. (London), Ser. A, Vol. 204, 1950, p. 309.

28. G. A. Lenning, C. M. Craighead, and R. I. Jaffee, "Constitution and Mechanical Properties of Titanium-Hydrogen Alloys," Trans. TMS-AIME, Vol. 200, 1954, p. 367.

29. L. W. Berger, D. N. Williams, and R. I. Jaffee, "Hydrogen in Titanium-Aluminum Alloys," Trans. TMS-AIME, Vol. 212, 1958, p. 509.

30. J. D. Boyd, "Deformation-Assisted Nucleation of Titanium Hydride in an Alpha-Beta Titanium Alloy," Paper presented at the International Conference on Titanium, London, England, May, 1968.

31. C. M. Craighead, G. A. Lenning, and R. I. Jaffee, "Nature of the Line Markings in Titanium and Alpha Titanium Alloys," Trans. TMS-AIME, Vol. 194, 1952, p. 1317.

32. D. N. Williams, "Report on Hydrogen in Titanium and Titanium Alloys," Titanium Metallurgical Laboratory Report No. 100, Battelle Memorial Institute, Columbus, Ohio, May, 1958.

33. M. J. Blackburn and J. C. Williams, "The Preparation of Thin Foils of Titanium Alloys," Trans. TMS-AIME, Vol. 239, 1967, p. 287.

34. G. Sanderson and J. C. Scully, "Hydride Formation in Thin Foils of Dilute Ti-Al Alloys," Trans. TMS-AIME, Vol. 239, 1967, p. 1883.

35. L. D. Jaffe, "Metallographic Identification and Crystal Symmetry of Titanium Hydride," Trans. TMS-AIME, Vol. 206, 1956, p. 861.

36. H. L. Yakel, Jr., "Thermocrystallography of Higher Hydrides of Titanium and Zirconium," Acta Crystallographica, Vol. 11, 1958, p. 46.

37. T. S. Liu and M. A. Steinberg, "The Mode of Hydride Precipitation in Alpha-Titanium Alloys," Trans. Am. Soc. Metals, Vol. 50, 1958, p. 455.

38. J. C. Williams and M. J. Blackburn, "The Identification of a Non-Basal Slip Vector in Titanium and Titanium-Aluminum Alloys," Physica Status Solidi, Vol. 25, 1968, p. K1.

39. M. J. Blackburn, "Relationship of Microstructure to Some Mechanical Properties of Ti-8Al-1V-1Mo," Trans. Am. Soc. Metals, Vol. 59, 1966, p. 694.

40. T. R. Beck and M. J. Blackburn, "Stress Corrosion Cracking of Titanium Alloys," American Institute of Aeronautics and Astronautics, Vol. 6, 1968, p. 326.

41. A. R. Troiano, "Embrittlement by Hydrogen and Other Interstitials," Metals Progress, Vol. 77, 1960, p. 112.

42. D. N. Williams and R. I. Jaffee, "Relationship Between Impact and Low-Strain-Rate Hydrogen Embrittlement of Titanium Alloys," J. Less-Common Metals, Vol. 2, 1960, p. 42.

43. H. H. Uhlig, "An Evaluation of Stress Corrosion Cracking Mechanisms," Paper presented at the Conference on the Fundamental Aspects of Stress Corrosion Cracking, Columbus, Ohio, September, 1967.

44. B. F. Brown, "The Application of Fracture Mechanics to Stress-Corrosion Cracking," Metallurgical Reviews, Vol. 13, 1968, p. 171.

45. M. H. Peterson, B. F. Brown, R. L. Newbegin, and R. E. Groover, "Stress Corrosion Cracking of High Strength Steels and Titanium Alloys in Chloride Solutions at Ambient Temperature," Corrosion, Vol. 23, 1967, p. 142.

46. J. M. Kraft, "Role of Local Dissolution in Corrosion-Assisted Cracking of Titanium Alloys," Naval Research Laboratory Progress, Vol. 6, 1965, p. 6.

47. N. G. Feige and T. Murphy, "Fracture Behavior of Titanium Alloys in Aqueous Environment," Metals Engineering Quarterly of the Am. Soc. Metals, Vol. 53, 1967, p. 53.

48. J. C. Scully, "Kinetic Features of Stress-Corrosion Cracking," Corrosion Science, Vol. 7, 1967, p. 197.

49. J. C. Williams and M. J. Blackburn, Private Communication.

50. B. F. Brown and C. D. Beachem, "A Study of the Stress Factor in Corrosion Cracking by Use of the Pre-Cracked Cantilever Beam Specimen," Corrosion Science, Vol. 5, 1965, p. 745.

51. G. P. Rauscher, Private Communication.

52. B. D. Cullity, Elements of X-ray Diffraction, Addison-Wesley Publishing Company, Reading, Massachusetts, 1956.

53. A. T. Churchman, "Determination of the Orientation of Single Crystals of Titanium," Metallurgia, Vol. 48, 1953, p. 50.

54. A. Phillips, V. Kerlins, and B. V. Whiteson, "Electron Fractography Handbook," Air Force Materials Laboratory Technical Report ML-TDR-64-416, Wright-Patterson Air Force Base, Ohio, January, 1965.

55. G. Thomas, Transmission Electron Microscopy of Metals, John Wiley & Sons, Inc., New York and London, 1962.

56. S. Fujishiro and H. L. Gegel, "Calculated Zone Axis and the Standard Electron Diffraction Patterns for Titanium," J. Less-Common Metals, Vol. 14, 1968, p. 467.

57. P. B. Hirsch, A. Howie, R. B. Nicholson, D. W. Pashley, and M. J. Whelan, Electron Microscopy of Thin Crystals, Plenum Press, New York, 1965.

58. Chemical Analysis of Metal: Sampling and Analysis of Metal Bearing Ores, Part 32 (Vol. 32), American Society for Testing Materials Standards, 1968.

59. V. Weiss and S. Yukawa, "Critical Appraisal of Fracture Mechanics," Fracture Toughness Testing, American Society for Testing Materials, Special Technical Publication No. 381, 1965, p. 1.

60. J. C. Williams, R. R. Boyer, and M. J. Blackburn, "The Influence of Microstructure on the Fracture Topography of Titanium Alloys," Boeing Company, Document D6-23622, Renton, Washington, June, 1968.

61. G. Sandoz, "Subcritical Crack Propagation in Ti-8Al-1Mo-1V Alloy in Organic Environments, Salt Water, and Inert Environments," Paper presented at the Conference on the Fundamental Aspects of Stress Corrosion Cracking, Columbus, Ohio, September, 1967.

62. R. M. N. Pelloux, Private Communication.